C.P. No. 1203

MINISTRY OF DEFENCE (PROCUREMENT EXECUTIVE)

AERONAUTICAL RESEARCH COUNCIL

CURRENT PAPERS

The Unsteady Response of an Axial Flow Compressor with a Distorted Inlet Flow

By

H. Mokelke, Dipl.-Ing.

University of Cambridge

Department of Engineering

LONDON. HER MAJESTY'S STATIONERY OFFICE

1972

75p net

C.P. No.1203*

October, 1970

THE UNSTEADY RESPONSE OF AN AXIAL FLOW COMPRESSOR WITH A DISTORTED INLET FLOW

- by -

H. Mokelke, Dipl.-Ing.

University of Cambridge

Department of Engineering

SUMMARY

A 4-stage axial flow compressor with a hub/tip ratio of 0.8 is investigated first with a 60°-square wave inlet distortion, then with two asymmetric spoiler configurations which are mirror images of each other. By measuring the total pressures, static pressures and yaw angles behind each stage, the development of the distortion is followed through the compressor.

---

* Replaces ARC32 372

List of Contents

Notation

Symbols

c	fluid velocity
c_x	axial fluid velocity
c_t	tangential fluid velocity
c_L	lift coefficient
f	oscillatory frequency, cps
D	drag force
F_r	resultant force
F_t	tangential blade force
F_x	axial blade force
i	incidence angle, deg.
i_g	geometric incidence angle, deg.
i_s	stalling incidence angle, deg.
k	reduced frequency parameter
L	lift force

1/

Notation (contd.)

l	rotor blade chord length,
P	total pressure
ΔP_R	total pressure rise across a rotor
p	static pressure
R_e	Reynolds number
s	rotor blade spacing
u	blade speed at mean diameter
w_m	relative vector mean velocity
$\left(\frac{\Delta P}{\rho u^2}\right)_{ov}$	overall total pressure rise coefficient
$(c_x/u)_{ov}$	overall flow rate; obtained from airmeter measurements
α	absolute air angle, deg.
β	relative air angle, deg.
$\eta_R = \frac{\Delta P_R/\rho}{u\Delta c_t}$	rotor efficiency
θ	circumferential location, deg.
ν	circumferential displacement of mean streamline between planes 2 and 4, deg.
ρ	air density
$\sigma = l_g/i_s$	incidence angle parameter
IGV	inlet guide vanes
OGV	outlet guide vanes
LE	leading edge
TE	trailing edge

Subscripts

1	location of plane at inlet
x	axial
t	tangential

m /

Notation (contd.)

m	vector mean
ov	overall
I	at rotor inlet
II	at rotor outlet
III	at stator inlet
IV	at stator outlet

Superscripts

-	circumferential average

1. Introduction

It has long been realized that axial compressors in aircrafts or other installations are frequently subjected to considerable inlet flow distortions. The general effect of these disturbances is to decrease the overall pressure rise and to generate premature compressor stall. Additionally, disturbances may persist right through the compressor and cause local overheating in a following combustion system. A simple way to simulate distorted inlet flows for testing purposes is to install distortion screens (made of wire gauze or similar material) upstream of the compressor. Uniform screen segments will generate square-wave distortions and although experiments with this perturbation type have already been performed (see for example Refs.4, 6 and 9) a 60°-square wave inlet flow distortion has been investigated in the first part of the experimental program reported in this paper. Particular care has been taken to obtain detailed interstage traverse data in order to study the alteration in shape of the distortion as it passes through the compressor.

In Ref.1, Carta suggests two hypothetical inlet distortions expressed as variations of relative rotor incidence angle with circumferential location (see Fig.3). The first distortion (referred to as forward traverse) was designed to produce a rapidly increasing and then a slowly decreasing incidence angle. The second distortion (referred to as backward traverse) was reversed but otherwise identical. Both perturbations have been further specified in such a way that the actual incidence angles exceed the quasi-steady stalling incidence angle over a considerable part of the circumference. Each of these two hypothetical incidence-circumferential location curves were converted by Carta into three different lift coefficient-circumferential location plots by:

(i) introducing empirical quasi-steady data (obtained from a single airfoil, see Fig.2)

(ii) using the unsteady potential flow theory of Theodorsen[8].

(iii) applying empirical unsteady data found on a single oscillating airfoil. (An example for one oscillatory frequency has been reproduced in Fig.2)

His results (see Fig.4a and 4b) show, as expected, that the lift coefficient curves obtained from empirical quasi-steady data are identical for the forward and backward traversed case, respectively. In the case where unsteady potential flow theory has been used, the magnitude of the corresponding lift coefficients is higher over the whole circumference than that obtained from empirical data. This result may have been expected since the theory does not predict any stalling phenomena. Further, the lift coefficients are fairly similar to one another, whereas the lift coefficient curves obtained from the introduction of unsteady empirical data show significant difference for the forward and backward traversed cases.

In the second part of the experimental program reported in this paper, the above described hypothetical disturbances have been replaced by forward and backward asymmetric triangular total pressure inlet distortions which were tested for a high and low flow rate. From these experiments Carta's results are confirmed except for two aspects discussed later.

2. Experimental Apparatus and Instrumentation

The experimental apparatus is a 4-stage low speed axial flow compressor (see Fig.1). It has a hub/tip ratio of 0.8, a mean radius of 6.3 inches and consists of inlet guide vanes, 4 identical stages and outlet guide vanes. Apart

from/

from the axial clearance between the TE of the last stator and the LE of the OGVs (which is 3.30"), all gaps between the blade rows have the same width of 0.54". The rotor and stator blade rows are identical and all blades (including IGVs and OGVs) are untwisted, have a constant section and possess a circular camber line.

Further details of the blading are given in the following table.

	IGV	rot./stat.	OGV
Camber angle, deg.	15	40	20
Stagger angle, deg.	-5.5	20	5
s/l at mid-height	0.59	0.88	1.18
Chord length (in.)	1.00	0.70	0.70
Number of blades	67	64	48
t/l in per cent	10	10	10
Base profile	C5	C5	C5

Five Fecheimer 3-hole-probes are lined up in the planes 2,4,6,8,10. They are installed at circumferential locations mid-way between the blade wakes of two adjacent upstream stator blades. Additionally a Kiel probe is installed 1.9" upstream of the LE of the IGVs (plane 1) and a wedge probe 2.3" downstream of the last stator (plane 11). The wedge probe is designed to record static pressure as well as total pressure. All probes measure the flow at mid-height position.

Outer wall static pressure tappings are installed in all planes except plane 11, where the pressure is taken from the wedge probe.

A support screen of a uniform eight meshes per inch is mounted in a rotatable ring at a distance of 5" or 0.8 compressor mean radii upstream of the inlet guide vanes. It may be turned through any desired angle from outside during the test, using a gear drive.

3. Tested Circumferential Spoiler Configurations

A 60° gauze segment with a density of 60 mesh/inch is attached to the support screen and creates the first inlet flow distortion investigated.

In addition an asymmetric triangular inlet distortion, extended over 180°, is established by installing 9 gauze segments each of 20° in order of decreasing gauze density. The reversed asymmetric triangular inlet distortion is created by rearranging the gauze segments in increasing order of gauze density. In Fig.7 the total pressure inlet distortions are presented schematically. The axis of symmetry is taken at a circumferential position of 150° to aid clarity in the presentation of results.

4. Test Procedure

In all tests the compressor was run at approximately 2980 r.p.m. which corresponds to a mean wheel speed of 165 ft/sec. The Reynolds number based on this speed and on the blade chord is then $R_e = 0.6 \times 10^5$.

The total and static pressure profiles for each spoiler configuration and flow rate were measured in planes 1,2,4,6,8,10 and 11. All pressures were related to the mean total pressure $\bar{P}_1$ at plane 1 and normalized using the dynamic pressure ρu^2 based on the mean wheel speed.

The flow angles were measured by balancing the instrument static pressures. No measurement of flow angle was obtained in plane 1 since only a Kiel probe had been installed.

In plane 1, therefore, the velocity (and not the axial velocity as in all other planes) is presented. Apart from plane 11, where a calibrated instrument static pressure was recorded, all velocities are based on the outer wall static pressures and are normalized using the mean wheel speed.

5. Discussion of Results

5.1 The square wave spoiler configuration

The 60°-square wave inlet distortion was first investigated for a high flow rate, $(c_x/u)_{ov} = 1.08$, see Fig.8.

As may be seen from Fig.9, the total pressure profiles in plane 1 and 2 are almost identical, which indicates that the inlet guide vanes have little effect on the total pressure distortion. The small irregularities seen in the inlet profiles are due to non-uniformities in the support screen.

In plane 4, behind the first stage, an alteration of the shape of the distortion has already taken place. The right hand part of the wake has attenuated more rapidly than the left hand part. This effect is repeated in planes 6 and 8 so that the shape of the total pressure profiles in these planes has become asymmetric. Fig.9 further demonstrates a good attenuation of the perturbations and a certain degree of shift in the direction of rotation.

In Fig.10 it is shown how the initially symmetric static pressure distortion is amplified from plane 1 to plane 2 and has altered its shape to an asymmetrical one. By following the static pressure profiles through the compressor it can be seen that they develop an even more asymmetrical shape than do the corresponding total pressure profiles.

The wake static pressure recorded in planes 10 and 11 is slightly higher than that over the rest of the circumference, and this is associated with a divergence of the wake streamlines, a phenomenon qualitatively predicted by Pearson and McKenzie in Ref.5. It is still possible for the static pressure rise across the outlet guide vanes to be consistent with uniform exit static pressure which is one of the main assumptions of the compressor-in-parallel theory (see Refs.2,3 and 5).

The flow angle profiles measured in the various planes are presented in Fig.11.

The velocity profile in plane 1 and axial velocity profiles in all other planes are shown in Fig.12. It is easily verified from these profiles that a certain degree of circumferential crossflow into the wakes takes place. Due to the higher static pressure gradients in the front stages, the amount of crossflow is higher here than in the rear stages. It may also be noted that the flow rate obtained by circumferentially averaging the axial velocities in any plane is higher than the overall flow rate, determined from airmeter measurements (between 16% in plane 2 and 23% in plane 10). This result may be expected since the overall flow rate represents an average of the whole annulus thus including

the/

the effect of wall boundary layers. Fig.12 further shows the (uniform) velocities in planes 1 and 11 at which the undistorted compressor would stall (see section 5.3). It may be noticed that the velocity of the perturbed flow at inlet and outlet does not fall below these steady-state stalling flow rates.

The above mentioned observation that the initially symmetrical total and static pressure disturbances develop an asymmetrical shape as the flow passes through the compressor may be explained as follows: If a compressor is subjected to a distorted inlet flow, significant tangential velocity perturbations (circumferential crossflow) will develop as the flow approaches the compressor face. (A small amount of crossflow also exists between the blade rows within the compressor). These tangential velocity perturbations have the effect of increasing the flow angle on one side of the distortion and decreasing it on the other, thus producing an asymmetry in the curves even if it is assumed that the flow around the rotor blades adjusts itself instantaneously to the corresponding steady-state flow conditions.

It is believed, however, that in addition to this quasi-steady effect, the unsteady behaviour of the flow relative to the rotor blades is responsible for a considerable degree of the observed asymmetry. The reasons for saying this are:-

(i) The closely spaced IGVs will produce an almost uniform flow direction, thus considerably reducing the magnitude of the upstream tangential velocity perturbations. (In fact, disregarding crossflow within the compressor, it should be possible with very closely spaced inlet guide vanes to eliminate asymmetric steady effects altogether). At first glance an inspection of the non-uniform flow angle distribution behind the IGV blades (Fig.11) seems to contradict this. One has to bear in mind, however, that strong total pressure gradients are in existence in plane 2 which cause a systematic error in the flow angle measurements. It is therefore likely that the true flow angle variation behind the IGVs is much smoother than the measured one.

(ii) The theories which predict significant crossflow upstream of the compressor assume the distortion to be introduced infinitely far upstream of the compressor. For the case under consideration, however, the distortion has been introduced approximately 0.8 compressor mean radii upstream of the LE of the IGVs, thus allowing only a small axial distance for the crossflow to develop.

A quantitative assessment of how far the observed asymmetry may be explained by quasi-steady crossflow effects can only be obtained by applying a suitable theory such as the actuator disc analysis presented in Refs.3 and 4. (It should be noted that neither the compressor-in-parallel theory nor the 'distributed body force' analysis described in Ref.7 may be used to establish this). No attempt has been made in this report to perform such a calculation.

In the next experiment the same spoiler configuration as before was used. Contrary to the previous case, however, the compressor was working at a low flow rate, $(c_x/u)_{ov} = 0.79$, close to its abrupt stalling point.

The total pressure, static pressure, flow angle and velocity perturbations are presented in Fig.13,14,15 and 16.

Due to the lower flow rate the total pressure loss in the spoiler gauze segment is reduced and the inlet distortion is of smaller magnitude. The shape of the total pressure profiles is again altered considerably through the compressor. The amplitude of the distortion, however, is almost the same in all planes, so that an attenuation in fact does not take place. The shift angle of the profiles in the direction of rotation has increased compared with that of

the/

the previous experiment. This will be at least partly due to the higher mean swirl of the absolute flow leaving a rotor when the compressor is working at a low flow rate. Fig.13 also shows large circumferential fluctuations in total pressure over a small region where the rotor blades leave the wake. The total pressure rise across each stage is smaller in this region than elsewhere.

In planes 1 and 2 the static pressure profiles are strongly distorted over the whole circumference but attenuate rapidly as the flow passes through the compressor. In the rear stages they differ little from those obtained for the high flow rate.

The flow angle profiles in plane 4,6,8,10 show quite similar fluctuations to the total pressure profiles at the same circumferential location.

Although the axial velocity profiles (Fig.16) alter their shape through the compressor in a similar way to the high flow rate case, larger perturbations persist at the compressor exit. Fig.16 further shows that (contrary to the previous experiment) the velocity of the perturbed flow at inlet and outlet falls over a certain part of the circumference below the steady-state stalling flow rate. This result indicates that the rotor blades operate over some part of the circumference beyond their quasi-steady stalling limit which suggests that the above mentioned local disturbances in total pressure (at the trailing edge of the spoiled region) are a local rotor stalling phenomenon. It should also be noted that for quasi-steady behaviour of the blades one would expect corresponding fluctuations on the left hand side of the distortion. A further investigation into this question has been carried out with the triangular inlet distortions and will be described in the following section.

5.2 The forward and backward asymmetric triangular spoiler configuration

This spoiler configuration has been investigated first for a high flow rate with $(c_x/u)_{ov} = 0.998$ and $(c_x/u)_{ov} = 1.015$ for the forward and backward traversed case respectively. (Ideally the flow rates should be identical but this was difficult to achieve).

The total pressure profiles are presented in Fig.17 and Fig.21. For the two cases the profiles attenuate quite similarly through the compressor, whereas the corresponding static pressure profiles, shown in Fig.18 and Fig.22, are somewhat less similar to one another.

The flow angle profiles correspond fairly well if possible measurement errors due to high total pressure gradients are borne in mind.

From Fig.20 and Fig.24 it may be seen that the axial velocity profiles are almost identical. It may further be noted that (apart from a small part of the circumference in pl.1) the velocity perturbations for both the forward and backward traversed case are above the steady-state stalling flow rates. Thus the rotor blades are not likely to produce any local stall and (since they also operate only with a moderately high mean blade loading) this case is comparable with Carta's result, obtained by using a hypothetical distortion in connection with Theodorsen's unsteady theoretical data.

The above observation that the forward and backward traversed disturbances show only minor differences in shape as the flow passes through the compressor may have the following reasons:-

(i) Circumferential crossflow (which acts in an opposite way on the two distortions) will be substantially reduced by the closely spaced inlet guide vanes.

(ii)/

(ii) The unsteady response of the rotor blades to the distortions is believed to be reasonably small ('potential flow unsteadiness'). This may be concluded from the similarity of Carta's unsteady theoretical lift coefficients for the forward and backward traversed disturbances (Fig.4a,b).

(iii) The forward and backward traversed total pressure distortions do in fact already show differences in shape upstream of the compressor, although the spoiler gauze configurations which created the perturbations were mirror images of one another. This is thought to be caused by the instalment of the spoiler gauze only 0.8 mean compressor radii upstream of the IGVs, so that the presence of the compressor itself may affect the screen total pressure drop by means of phenomena (i) and (ii) above. As already stated, however, for the high flow rate case these are small, and therefore their effect is not severe.

In the next experiment the compressor was operated at a low flow rate near its abrupt stalling point. For the forward traversed case, $(c_x/u)_{ov} = 0.765$, the total pressure distortions are presented in Fig.25. No irregularities in the profiles occur where the total pressure is rapidly decreasing. Also for the backward traversed case, Fig.29, $(c_x/u)_{ov} = 0.762$, no additional irregularities other than those due to the spoiler screen are noticeable over the range where the total pressure slowly decreases. For increasing total pressure the rapidity of change is important. In the forward traversed case total pressure irregularities of small amplitude are distributed over the whole region of slowly increasing total pressure. In the backward traversed case, however, larger total pressure disturbances occur at a circumferential location where the pressure is rapidly increasing. In both cases, these local disturbances in the total pressure, accompanied by a reduction in total pressure increase across a stage, may again (as for the 60°-square wave distortion investigated at a low flow rate) be interpreted as a local rotor stalling phenomenon. Thus if a 'short duration stall' is defined as a temporary drop in lift for a blade already working beyond the quasi-steady limit which is not predictable by an unsteady potential flow analysis, one may summarize as follows:

(i) No short duration stall could be observed over the region of either rapidly or slowly decreasing total pressure.

(ii) For the forward traversed case, short duration stall of relatively low magnitude occurs over the large region of slowly increasing total pressure.

(iii) For the backward traversed case short duration stall of a higher magnitude occurs over a small region where the total pressure increases rapidly.

In order to obtain a more quantitative comparison with Carta's results, an attempt has been made to determine the behaviour of the lift coefficient for a rotor blade of the first stage as it travels through the distorted and undistorted region. The way this has been achieved is described in the Appendix.

The solid lines in Fig.5a,b, referred to as 'low flow rate unsteady experimental', represent the lift coefficients for the forward and backward traversed case respectively. (The appropriate scales are shown on the left hand side of the diagrams). It may be seen from Fig.28 and Fig.32 that the rotor blades are operating over a substantial part of the circumference beyond the quasi-steady limit. The results are therefore comparable with the lift coefficients obtained by Carta from unsteady empirical data (see solid lines, Fig.4a,b).

The/

The dash-dot lines in Fig.4a,b, represent the lift variations obtained by Carta from Theodorsens unsteady potential flow theory (see Ref.8). No similar computation has been performed here. Instead, comparable lift coefficients have been determined from the experiments described above, where the compressor was operating at a high flow rate. These lift variations (represented by dash-dot lines in Fig.5a,b) have been superimposed on those obtained for the low flow rate in such a way that both coincide over a part of the undistorted region. (The scales are shown on the right hand side of the diagrams). In the following discussions they will be referred to as 'high flow rate-unsteady experimental'.

Firstly, consider Carta's result in Fig.4a. The unsteady empirical lift coefficient initially follows the unsteady theoretical curve almost to its maximal value but then breaks away sharply at about 130°, decreases rapidly and does not rejoin the level of the theoretical curve for a further 200°.

In Fig.5a, the 'low flow rate-unsteady experimental' response increases as the 'high flow rate-unsteady experimental' response increases but it breaks away shortly before the maximal value has been reached. It then decreases at a somewhat higher rate than the 'high flow rate-unsteady experimental' curve but rejoins it again at approximately 240°.

It may therefore be concluded that the forward traversed distortion produces stall which extends over a significant part of the circumference but with a magnitude less severe than demonstrated by Carta's results. An inspection of the total pressure profiles (at a location where the total pressure increases) in Fig.25, behind the second, third and fourth stages seems to indicate that the severity of stall in the rear stages is even lower than in the front stage.

Next consider Fig.4b, for the backward traversed distortion. As may be seen, the unsteady empirical lift curve follows the unsteady theoretical lift curve (although not quite to the maximal values) over the period of increasing lift, breaks away as it suddenly decreases, but rejoins the level of the theoretical lift shortly afterwards.

Similar behaviour is shown by the 'low flow rate-unsteady experimental' lift curve in Fig.5b, except that, after the sudden decrease, it remains substantially below the 'high flow rate-unsteady experimental' curve for more than 30 degrees of the circumference.

It may therefore be concluded that the backward traversed distortion is somewhat more detremental in respect of generating stall (at a location where the rotor blades are leaving the distortion) than Carta's results indicated.

Despite these differences there is a remarkable similarity between the unsteady behaviour of the empirical lift coefficients reported by Carta and those obtained here. This may be explained by comparing the corresponding reduced frequency parameters. The first harmonic component of the investigated triangular inlet distortion, with the circumferentially averaged relative vector mean velocity $\overline{w}_m$ (determined at mid-height in plane 2) chosen as the free stream velocity, yields a reduced frequency parameter of $k = 0.067$. This result almost coincides with the reduced frequency parameter of $k = 0.075$ obtained for the single airfoil, oscillating with a low frequency of 4 cps (see Fig.2). Higher oscillatory frequencies for the airfoil will be comparable with higher harmonic components of the disturbance. Remembering that the single airfoil tests provided Carta's unsteady empirical data these agreements may well explain the observed similarity of the lift coefficients.

After/

After these considerations of the unsteady stalling phenomenon on the the rotor blades it may be useful to compare again the shape of the forward and backward traversed triangular distortions. As may be seen from Fig.25 and Fig.29, the distortion profiles (for the compressor working at a low flow rate) are considerably less similar to one another than are the corresponding profiles for the high flow rate. This could be because of the following reasons:

(i) Circumferential crossflow (which affects the two distortions in opposite senses) may have a greater effect as can be estimated from the severity of the static pressure perturbations at compressor inlet.

(ii) The response of the rotor blades to the perturbation is of a more unsteady nature here than for the high flow rate case. Short duration stall of variable extent and magnitude superimposed on the milder 'potential flow unsteadiness' may be responsible for this result.

(iii) The effect of compressor proximity on screen pressure loss, described above for high flow rates, will be greater here since crossflow and unsteady response effects are correspondingly greater, tending to introduce a greater disparity between the two total pressure profile shapes before the compressor is even reached.

5.3 The performance of the compressor with and without inlet distortion

The overall performance of the undistorted and distorted compressor is shown in Fig.8. For the distorted compressor, the total pressure increase was determined from circumferentially averaging the total pressure profiles measured in planes 1 and 11. A similar procedure was applied for each point of the undistorted compressor characteristic. This was done because the support screen itself produced a slight perturbation due to small unavoidable non-uniformities in the wire gauze.

The figure shows that for the high flow rate the total pressure-rise coefficient for the 60°-square wave inlet distortion is of the same order as the undistorted coefficient. For the lower flow rate, however, it is substantially reduced, owing to the higher losses in the blade rows. (This result has also been obtained by Katz in Ref.4).

Similar behaviour is observed for the triangular distortion. For both the forward and backward traversed disturbance, the deterioration in total pressure rise coefficient increases as the flow rate decreases. The small difference between the two cases at the low flow rate may support the view that the forward traversed distortion produces unsteady rotor blade stall of relatively low magnitude over a long circumferential distance, whereas the backward traversed distortion shows the opposite tendency, generating stall of a higher magnitude over a short circumferential distance. Assuming similar stator losses for the forward and backward traversed case, these two different stall patterns could nevertheless have comparable effects on the circumferentially averaged total pressure increase across the compressor.

The onset of rotating stall for both the perturbed and unperturbed compressor was easily identified by the sudden change in sound and by the discontinuities in the pressure readings. For the undistorted case abrupt compressor stall was found to occur at $(c_x/u)_{ov} = 0.702$ which corresponds to a flow rate (at mid-height) in plane 1 and plane 11 of $c_x/u = 0.843$ and $c_x/u = 0.866$ respectively. These latter flow rates have been included in all

figures/

figures showing axial velocities in order to indicate the steady-state stalling flow rates for the various disturbances under consideration.

Abrupt compressor stall for the forward traversed perturbation was recorded at $(c_x/u)_{ov} = 0.740$ and for the backward traversed one at $(c_x/u)_{ov} = 0.736$. Thus the compressor stalling flow is almost the same for the two types of distortions.

A comparison with the unperturbed compressor, however, shows that a definite deterioration concerning the onset of compressor stall has occurred. This result differs from the one obtained by Katz in Ref.4 for a three-stage compressor where the inception of rotating stall was almost unaffected by the inlet disturbance. The reason could be that his inlet distortion attenuated very rapidly through the compressor so that the last stage, which was possibly responsible for the onset of rotating stall, operated in an almost uniform flow.

6. Conclusions

6.1 60°-square wave spoiler configuration

(a) For the compressor working at a high flow rate, the initially symmetric static pressure profile (and to a smaller extent also the total pressure profile) changes to an asymmetric shape as the flow passes through the compressor. Since the closely spaced inlet guide vanes will considerably reduce steady asymmetric effects it is likely that a substantial degree of the observed asymmetry is due to the unsteady 'potential flow' response of the rotor blades while these are passing through a distorted region.

(b) For the compressor working at a low flow rate, local irregularities and 'peaks' in total pressure at the trailing edge of the spoiled region have been interpreted as a local rotor stalling phenomenon (short duration stall).

6.2 Triangular spoiler configuration

(a) Forward and backward traversed asymmetrical inlet distortions, extending over 180°, show only minor differences in their developed shapes if the compressor works well away from its abrupt stalling point. These discrepancies might be explained by small circumferential crossflow effects together with a mild unsteady 'potential flow' blade response.

(b) The same spoiler arrangements as before, but investigated for a low flow rate, show that the differences in the forward and backward traversed profiles are substantially enlarged. Increased crossflow effects and a greater departure from quasi-steady conditions due to short duration stall are believed to be responsible for this result. Detailed consideration of this local rotor stalling phenomenon showed that little or no short duration stall occurred in regions of either rapidly or slowly decreasing total pressure. For the forward traversed case, short duration stall of a relatively low magnitude could be observed over the large region of slowly increasing total pressure. For the backward traversed case short duration stall of a higher magnitude occurs over a small region where the total pressure increases rapidly.

Acknowledgements

The test apparatus used belongs to the Derby and District College of Technology and the author expresses his gratitude for being allowed to use it for his experimental research program. The author also acknowledges the assistance of Professor J. H. Horlock and Dr. J. P. Gostelow, who supervised the work.

References/

References

No.	Author(s)	Title, etc.
1	F. O. Carta	Unsteady normal force on an airfoil in a periodically stalled inlet flow. J. of Aircraft, Vol.4, No.5, p.416. 1967
2	M. D. C. Doyle, S. L. Dixon and J. H. Horlock	Circumferential asymmetry in axial flow compressors. J. R. Aer. Sci. October, 1966
3	J. Dunham	Non-axisymmetric flows in axial compressors Cambridge University, Ph.D. Thesis 1962
4	R. Katz	Performance of axial compressors with asymmetric inlet flows. Guggenheim Jet Propulsion Centre, Cal. Inst. Tech. Report. 1958
5	H. Pearson and A. B. McKenzie	Wakes in axial compressors. J. R. Aero. Soc., Vol.63, No.583, p.415. 1959
6	F. Roberts, G. A. Plourde and F. Smakula	Insights into axial compressor response to distortion. AIAA Paper No.68-565. 1969
7	A. H. Stenning and G. A. Plourde	The attenuation of circumferential inlet distortion in multi-stage axial compressors. AIAA Paper No.67-415. 1967
8	T. Theodorsen	General theory of aerodynamic instability and the mechanism of flutter NACA Rept.496. 1935
9	R. C. Turner, J. Ritchie and C. E. Moss	The effect of inlet circumferential maldistribution on an axial compressor stage. ARC R. & M. No.3066. 1957

APPENDIX /

APPENDIX

If the lift coefficient for a rotor blade is defined as

$$c_L = \frac{L}{\rho/2 w_m^2 \, l} \qquad \ldots(1)$$

it is apparent that for a distorted flow this coefficient will be a function of the circumferential location, $c_L = c_L(\theta)$, since the lift as well as the relative vector mean velocity vary as the rotor blade passes through the distortion. From the vector diagram of the vector diagram of the blade forces in Fig.6, it may be deduced that

$$L(\theta) = F_x \sin\beta_m + F_t \cos\beta_m \qquad \ldots(2)$$

where

$$F_t = \frac{c_x/u}{\eta_R} s\Delta P_R \qquad \ldots(3)$$

and

$$F_x = \left(1 - \frac{1}{\eta_R} + \frac{1}{\eta_R}\frac{c_x}{u}\tan\beta_m\right) s\Delta P_R \qquad \ldots(4)$$

Thus

$$L = s\Delta P_R \left[\left(1 - \frac{1}{\eta_R}\right)\sin\beta_m + \frac{1}{\eta_R}\frac{c_x}{u}\frac{1}{\cos\beta_m}\right] \qquad \ldots(5)$$

With

$$w_m = \frac{c_x}{\cos\beta_m} \qquad \ldots(6)$$

it is found that

$$c_L = 2\frac{s}{l}\frac{\cos\beta_m}{c_x/u}\frac{\Delta P_R}{\rho u^2}\left[\left(1 - \frac{1}{\eta_R}\right)\frac{\sin\beta_m \cos\beta_m}{c_x/u} + \frac{1}{\eta_R}\right] \qquad \ldots(7)$$

Apart from the space/chord ratio all properties of Eqn.(7) are functions of the circumferential location and will be discussed below.

(i) The dimensionless axial velocity $c_x/u = f(\theta)$ in the plane 2 is known.

(ii) The rotor efficiency $\eta_R = f(\theta)$ can only be determined from measurements of the temperature increase across the rotor. It may, however, be assumed that its variation over the circumference is of the same order as the variation in overall compressor efficiency for the compressor operating with a triangular inlet flow distortion at the investigated high, medium and low flow rates. Since these variations are small compared with the variations of the other properties in Eqn.(7), the rotor efficiency may be regarded (in a first approximation) to be a constant. It is set equal to the overall compressor efficiency, calculated for the distortion under consideration.

(iii)/

(iii) The relative vector mean flow angle $\beta_m = f(\theta)$ is found from the relation

$$\tan\beta_m = \tfrac{1}{2}\left(\tan\beta_I + \tan\beta_{II}\right) \qquad \ldots(8)$$

The relative flow leaving angle β_{II} is assumed to be constant and equal to the absolute inlet flow angle α_I for the undistorted compressor. It should be noted that this can only be a rather rough approximation, at least for the case where the distorted compressor operates at a low flow rate with possible local stalling of the rotor blades. The relative flow inlet angle $\beta_I = f(\theta)$ is found from

$$\tan\beta_I = \frac{1}{c_x/u} - \tan\alpha_I$$

where $c_x/u = f(\theta)$ and $\alpha_I = f(\theta)$ have been determined in plane 2.

(iv) The total pressure difference $\Delta P_R = f(\theta)$ should be calculated from total pressure measurements taken immediately upstream and downstream of the rotor blade row 'contracted to a disc'. In fact, however, the total pressure readings have been taken slightly further upstream in plane 2 and considerably further downstream in plane 4 behind the adjacent stator blade row. In order to utilize these measurements two additional simplifications have been introduced.

First, the probe in plane 4 is installed mid-way between two stator blades thus being only subject to a small proportion of the upstream stator losses (since these are concentrated in the blade wakes). Stator losses are therefore ignored ($P_{III} = P_{IV}$). Secondly, small perturbation theory shows that the total pressure remains constant along mean streamlines which are regarded as identical to the streamlines for the undistorted compressor. The swirl angle ν of the mean flow is found (as indicated in Fig.6) from the absolute flow angles α_I and α_{III} for the undistorted compressor, from the assumption that $\beta_{II} = \alpha_I$, and from the circumferentially averaged flow rate (at mid-height) in plane 2 of the compressor for the inlet distortion under consideration.

By shifting the entire total pressure profile, measured in plane 4, against the direction of rotation by the swirl angle ν and then taking the difference to the total pressure profile determined in plane 2 the required property $\Delta P_R = f(\theta)$ is obtained

---

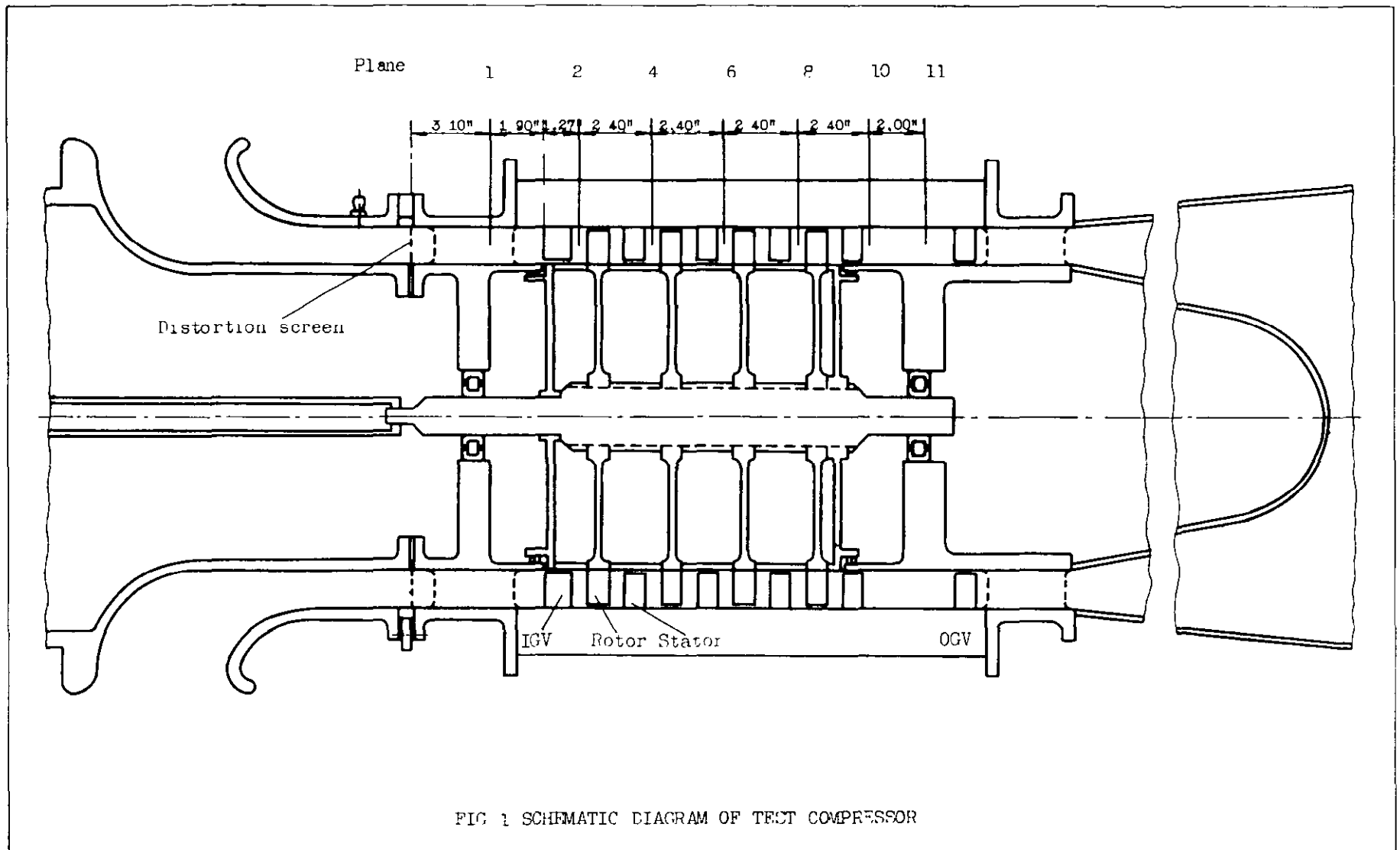

FIG 1 SCHEMATIC DIAGRAM OF TEST COMPRESSOR

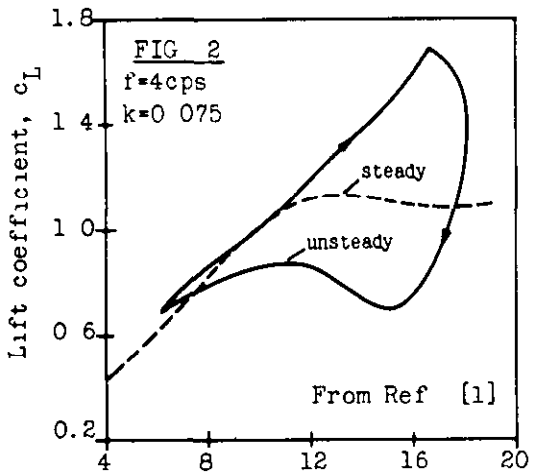

UNSTEADY LIFT LOOP

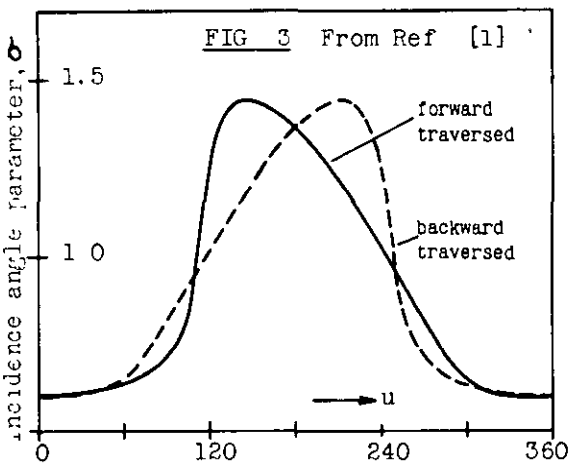

HYPOTHETICAL DISTORTION PROFILE

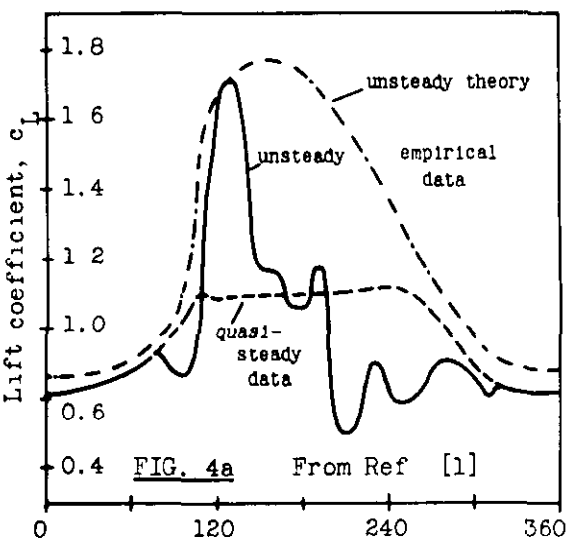

SINGLE AIRFOIL RESPONSE TO A FORWARD TRAV. DIST PROFILE

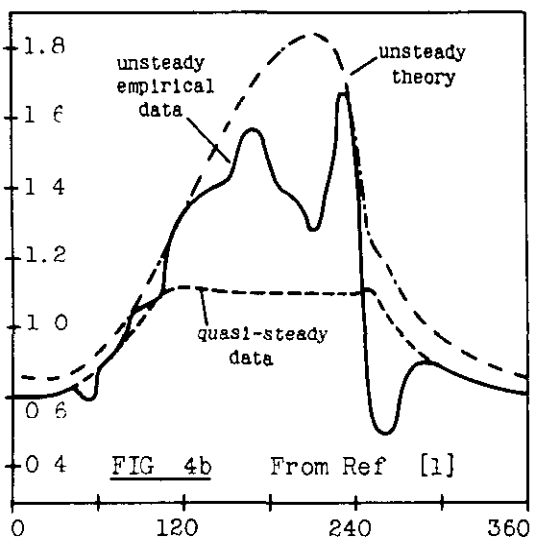

SINGLE AIRFOIL RESPONSE TO A FORWARD TRAV DIST. PROFILE

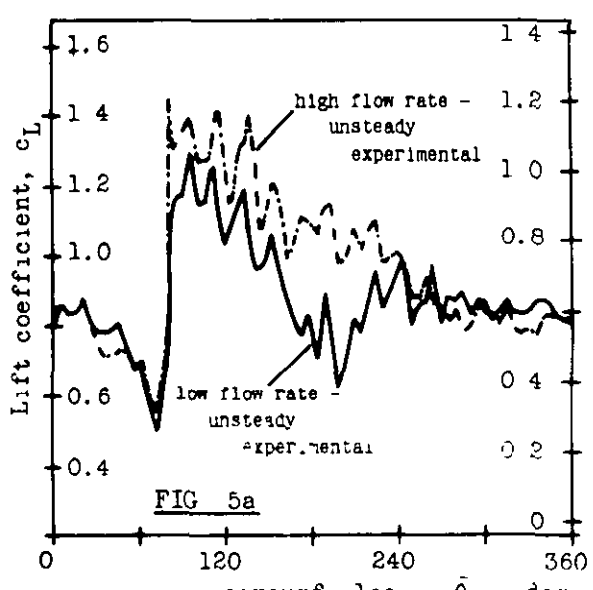

ROTOR BLADE RESPONSE TO A FORWARD TRAV DIST. PROFILE

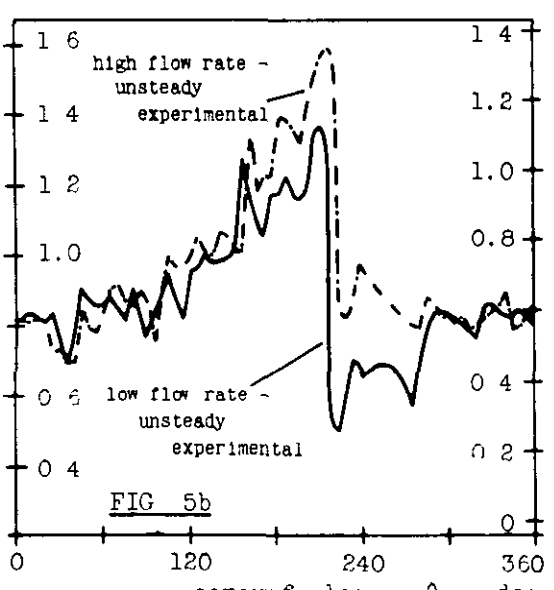

ROTOR BLADE RESPONSE TO A BACKWARD TRAV DIST PROFILE

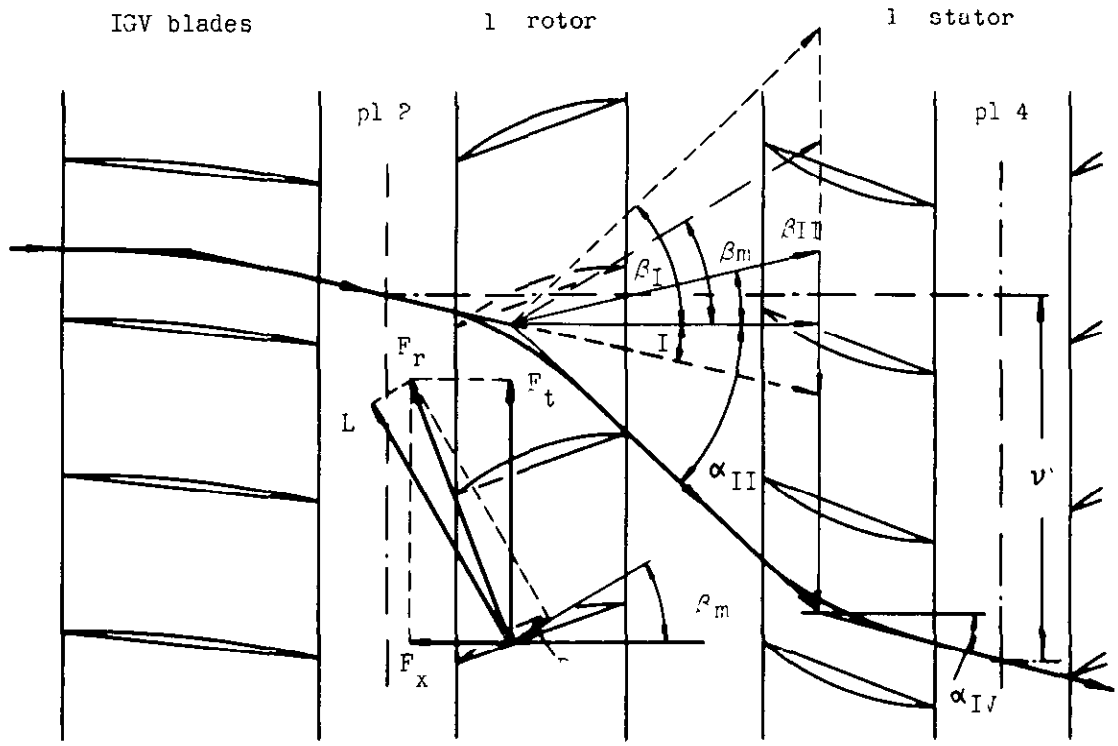

FIG 6 ESTIMATION OF MEAN SWIRL ANGLE BETWEEN PLANES 2 AND 4

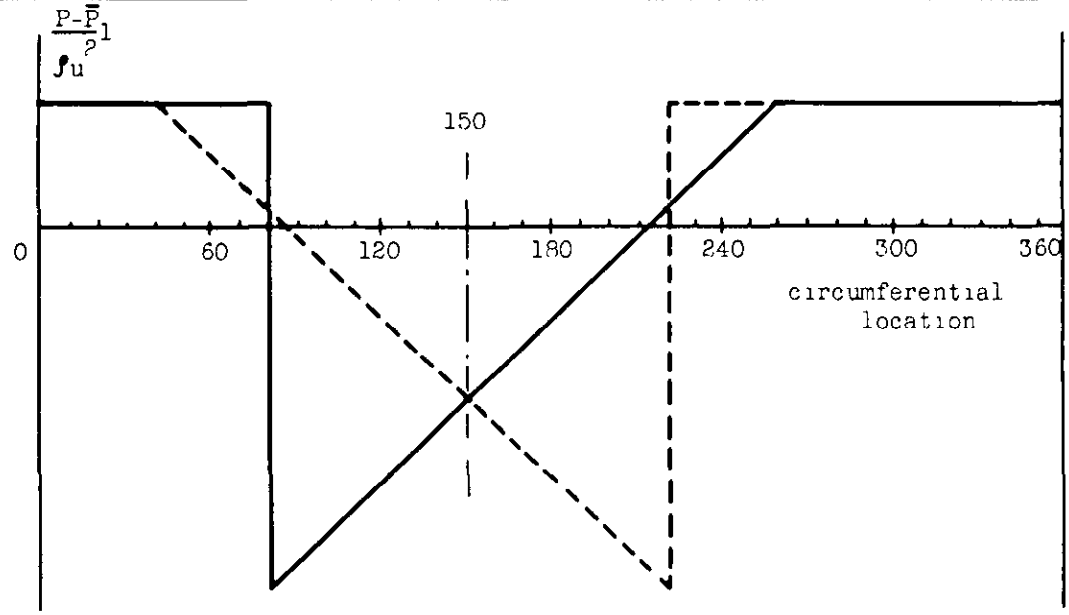

FIG 7 SCHEMATIC DIAGRAM OF ASYMMETRIC TRIANGULAR TOTAL PRESSURE INLET DISTORTIONS

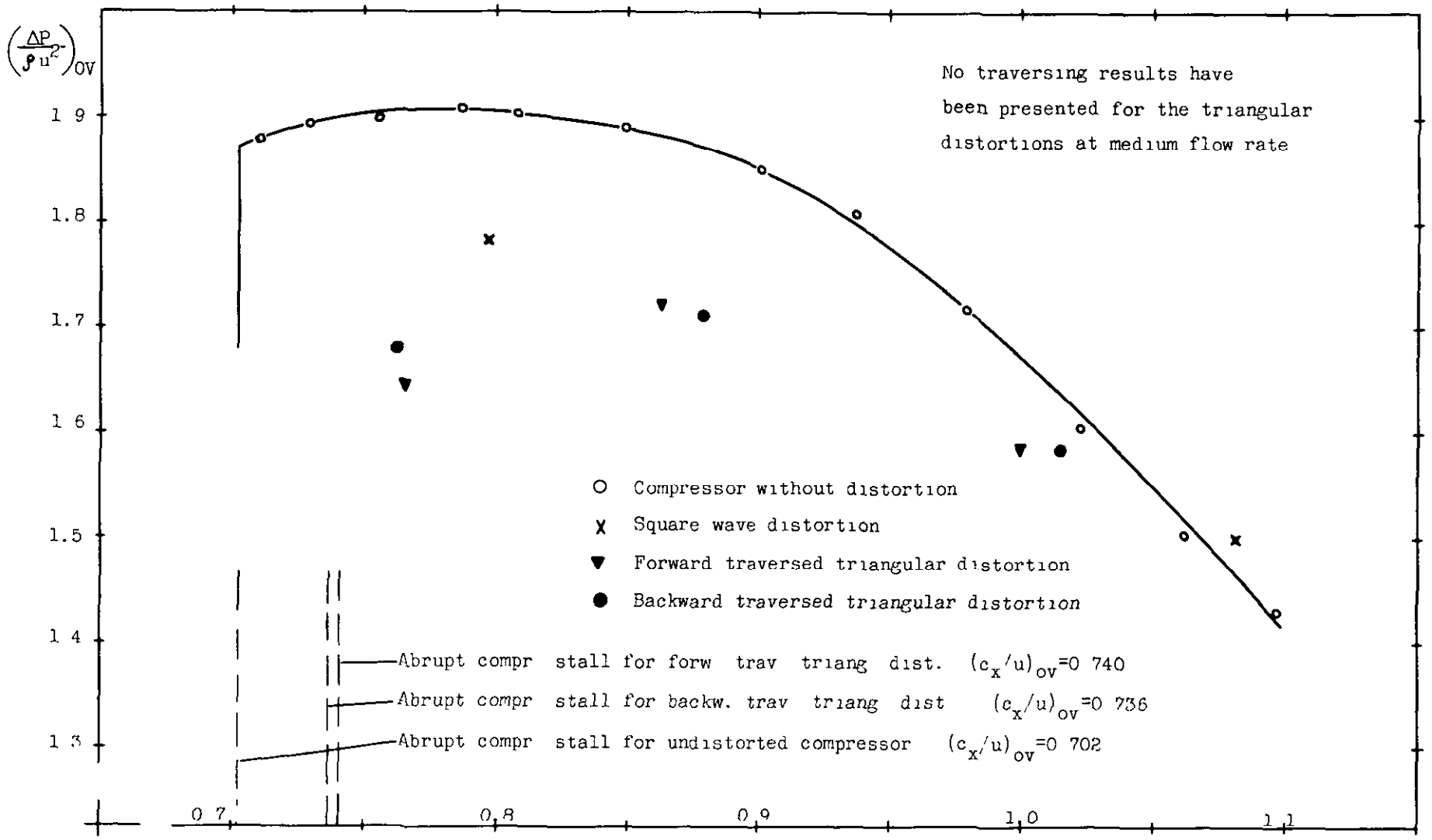

FIG 8 OVERALL TOTAL PRESSURE RISE COEFFICIENT FOR THE COMPRESSOR WITH AND WITHOUT INLET DISTORTIONS

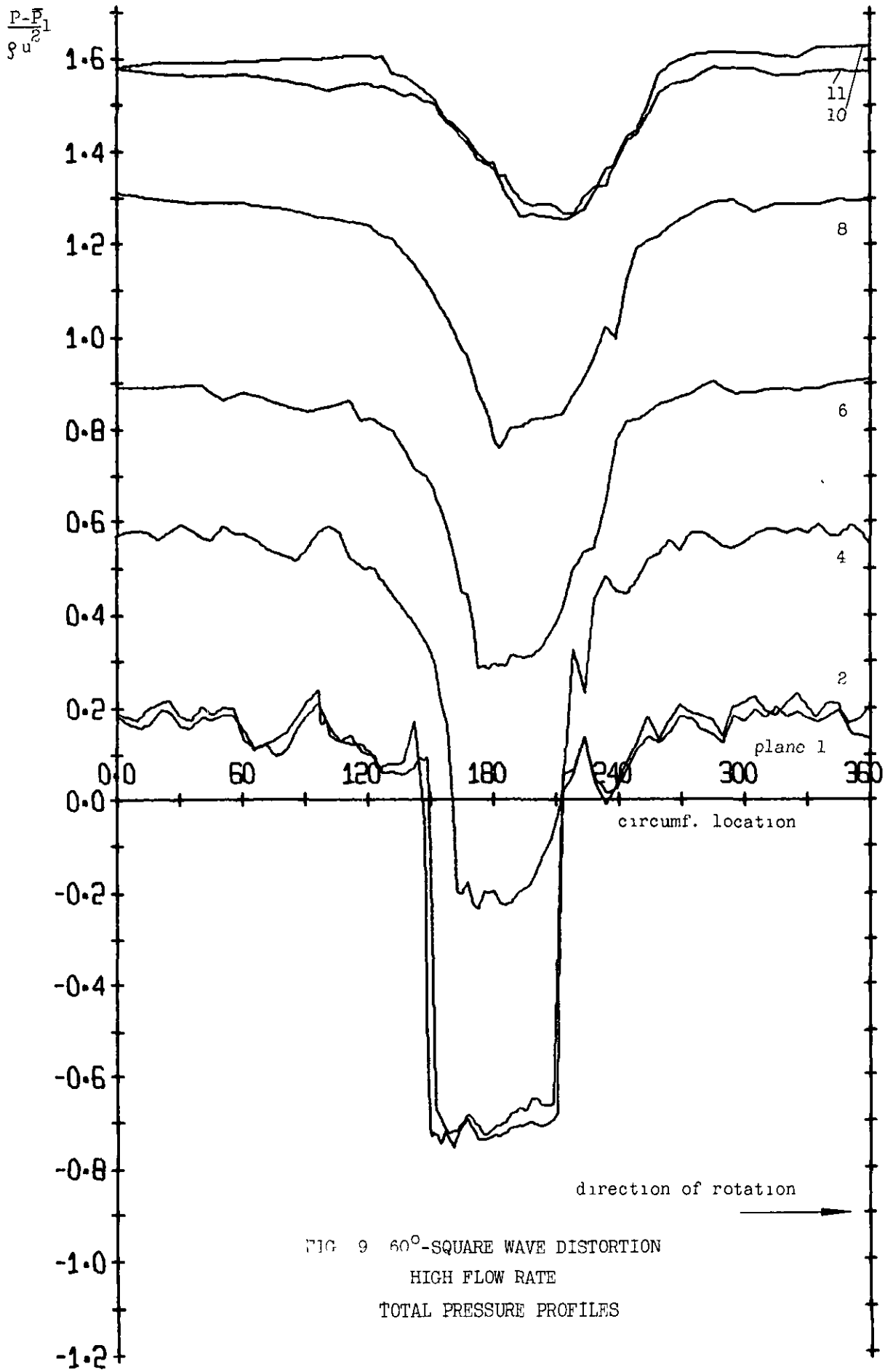

FIG 9 60°-SQUARE WAVE DISTORTION
HIGH FLOW RATE
TOTAL PRESSURE PROFILES

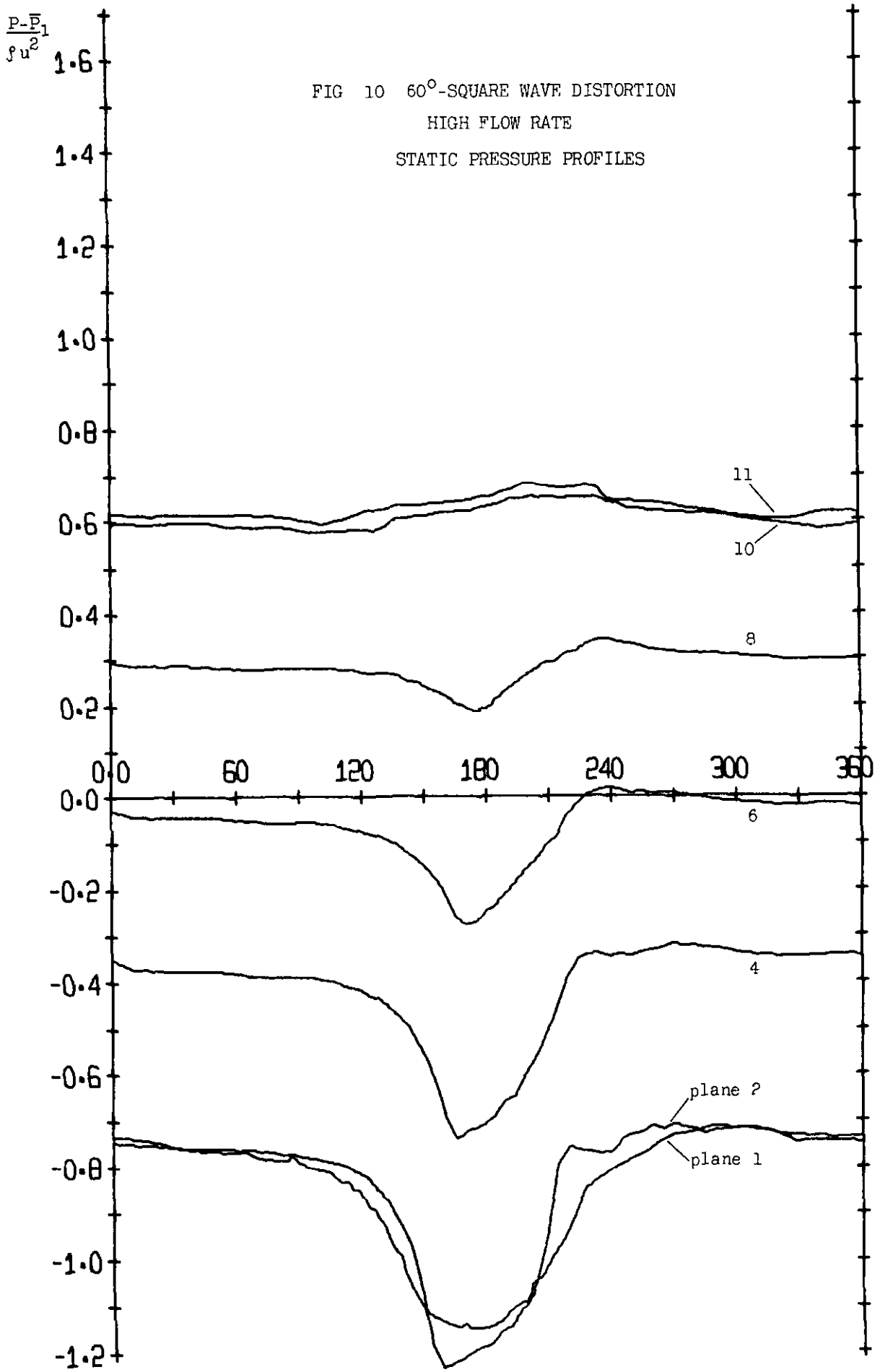

FIG 10 60°-SQUARE WAVE DISTORTION

HIGH FLOW RATE

STATIC PRESSURE PROFILES

FIG. 11 60°-SQUARE WAVE DISTORTION

HIGH FLOW RATE

FLOW ANGLES

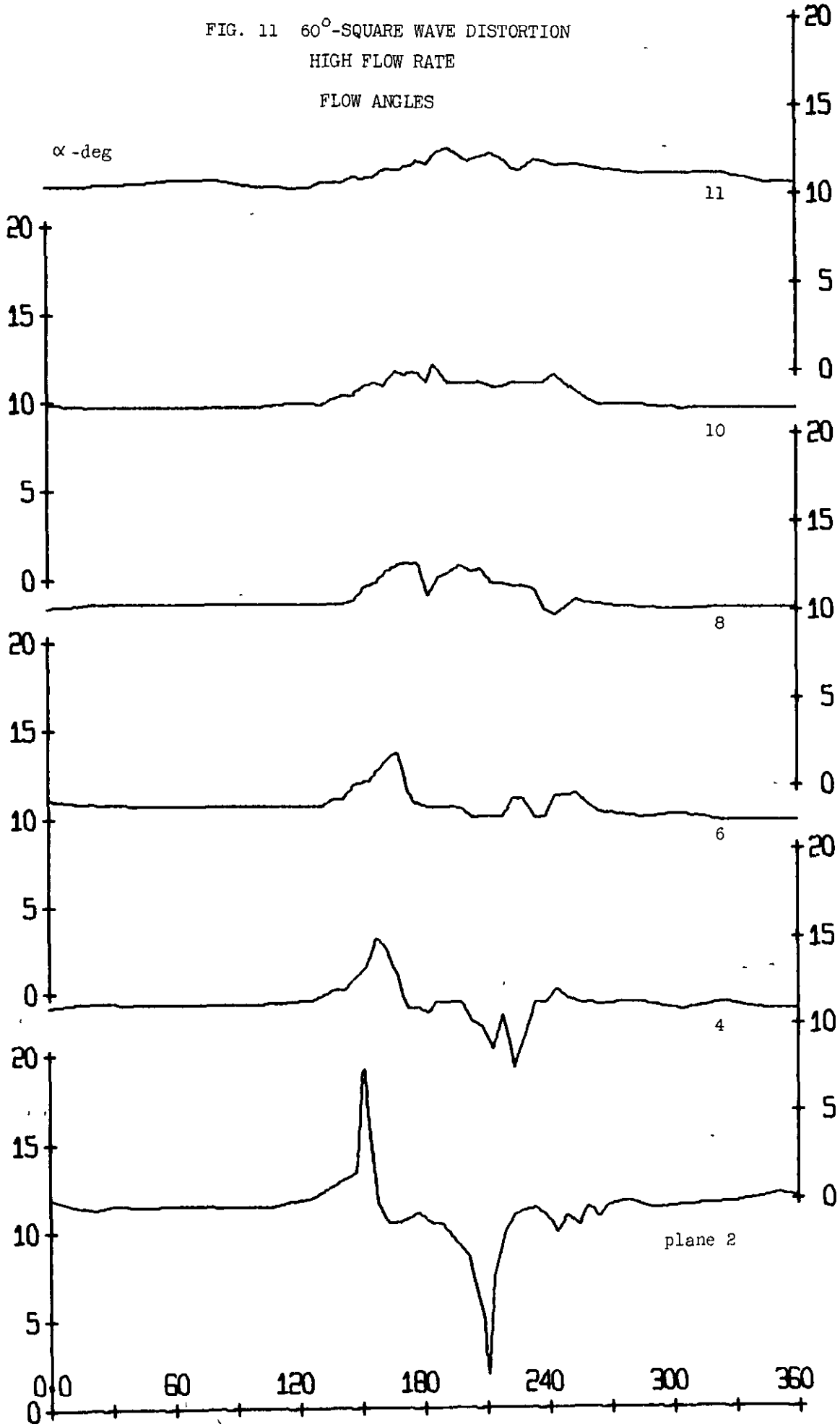

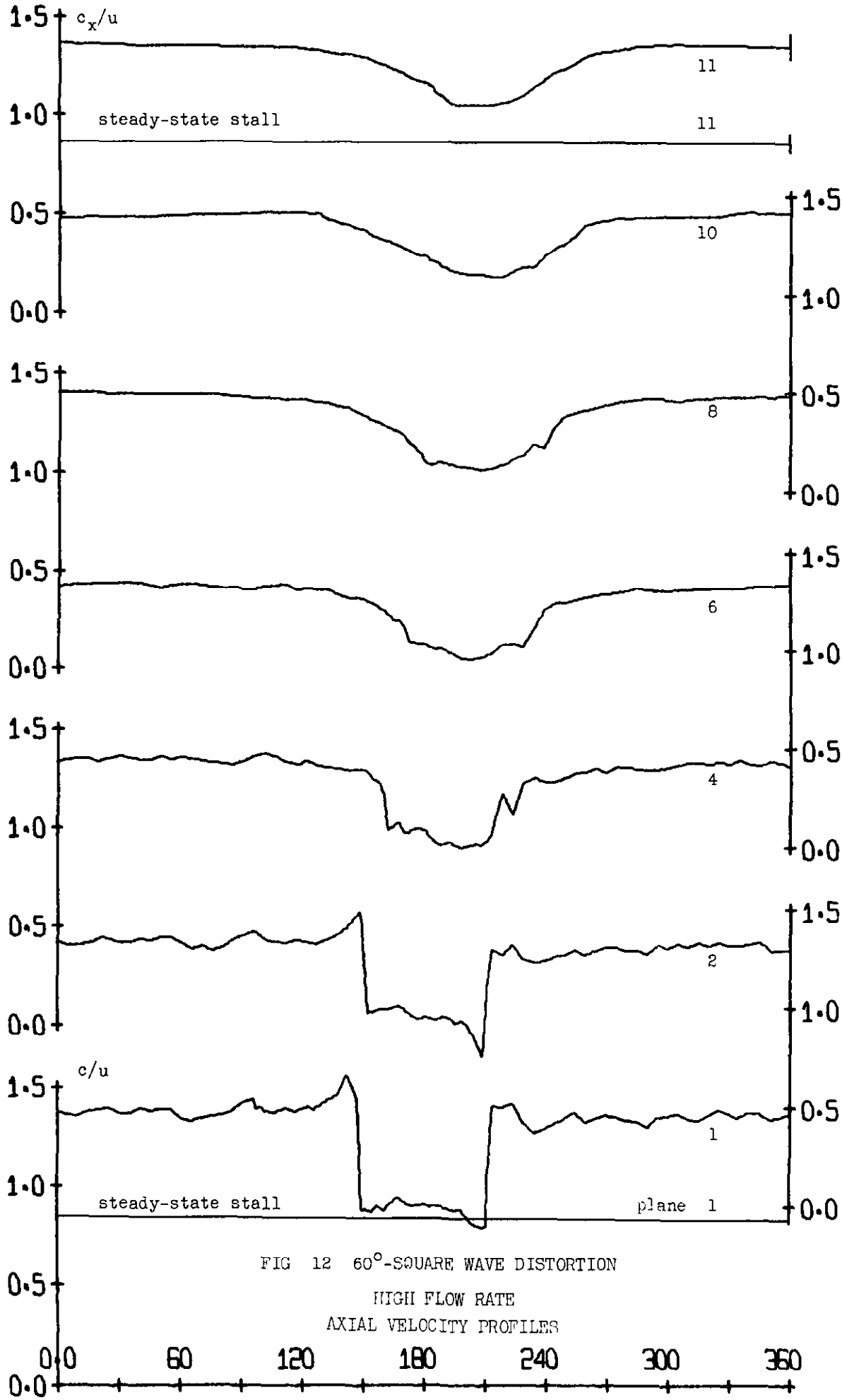

FIG 12 60°-SQUARE WAVE DISTORTION

HIGH FLOW RATE

AXIAL VELOCITY PROFILES

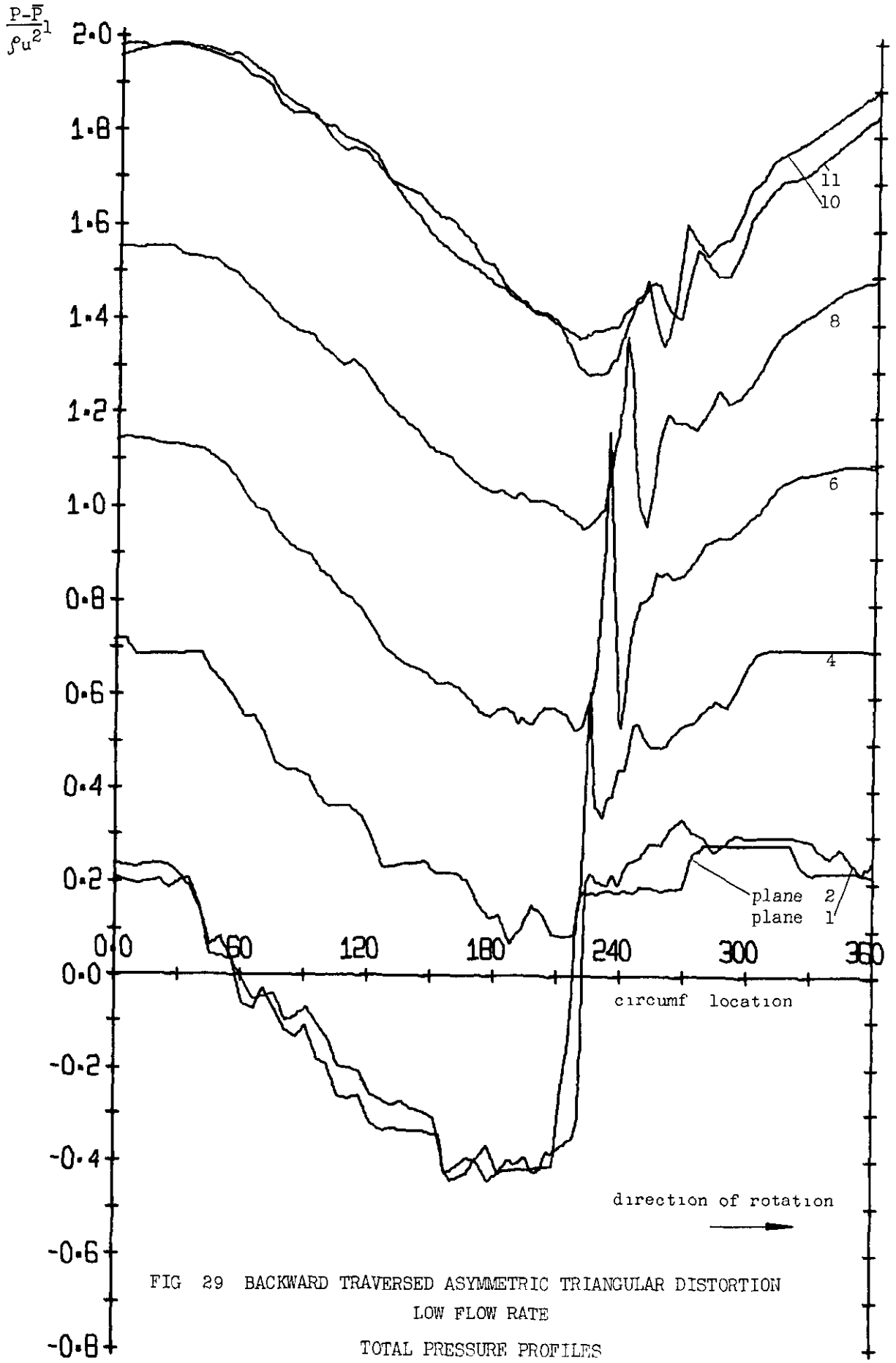

FIG 29 BACKWARD TRAVERSED ASYMMETRIC TRIANGULAR DISTORTION
LOW FLOW RATE
TOTAL PRESSURE PROFILES

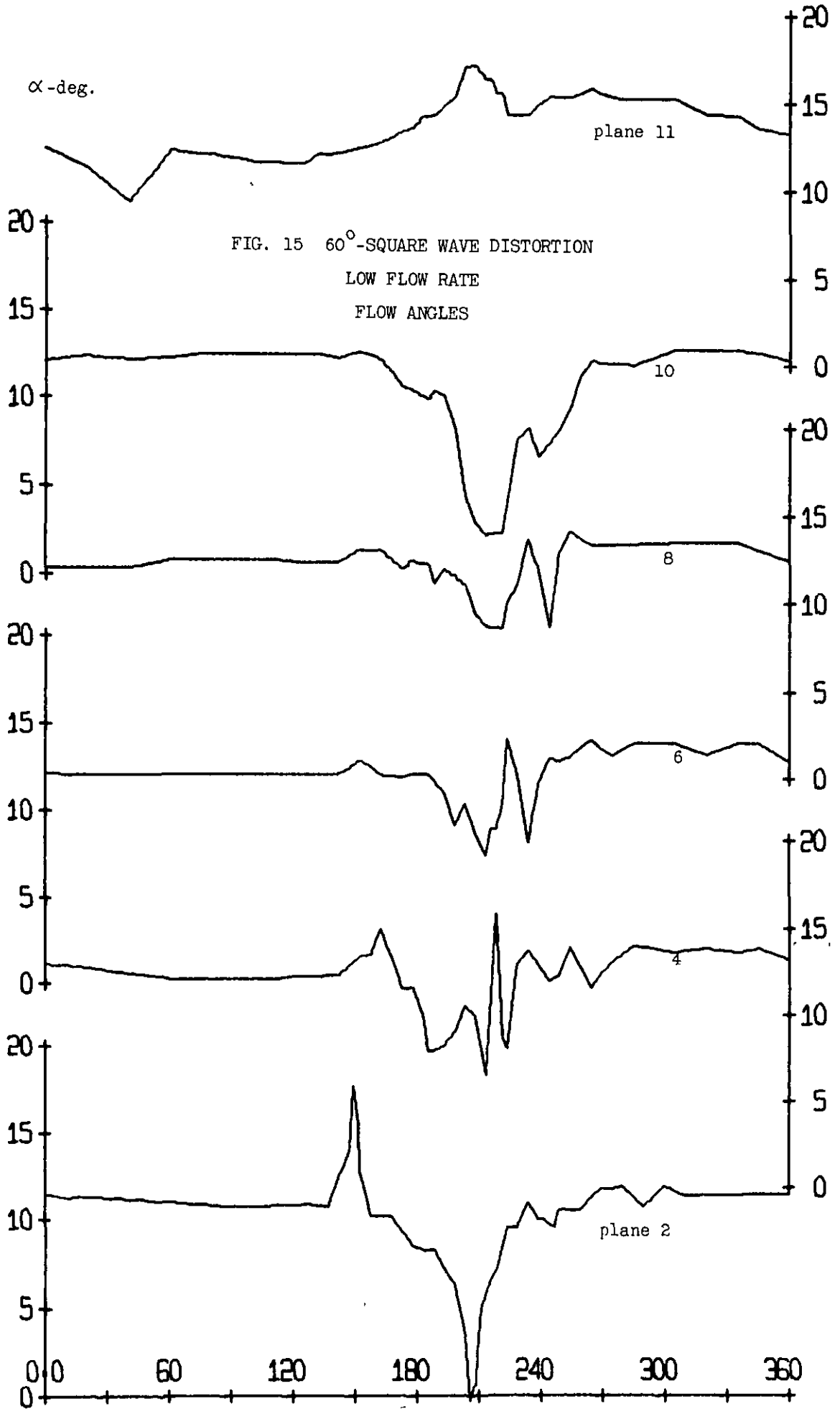

FIG. 15 60°-SQUARE WAVE DISTORTION
LOW FLOW RATE
FLOW ANGLES

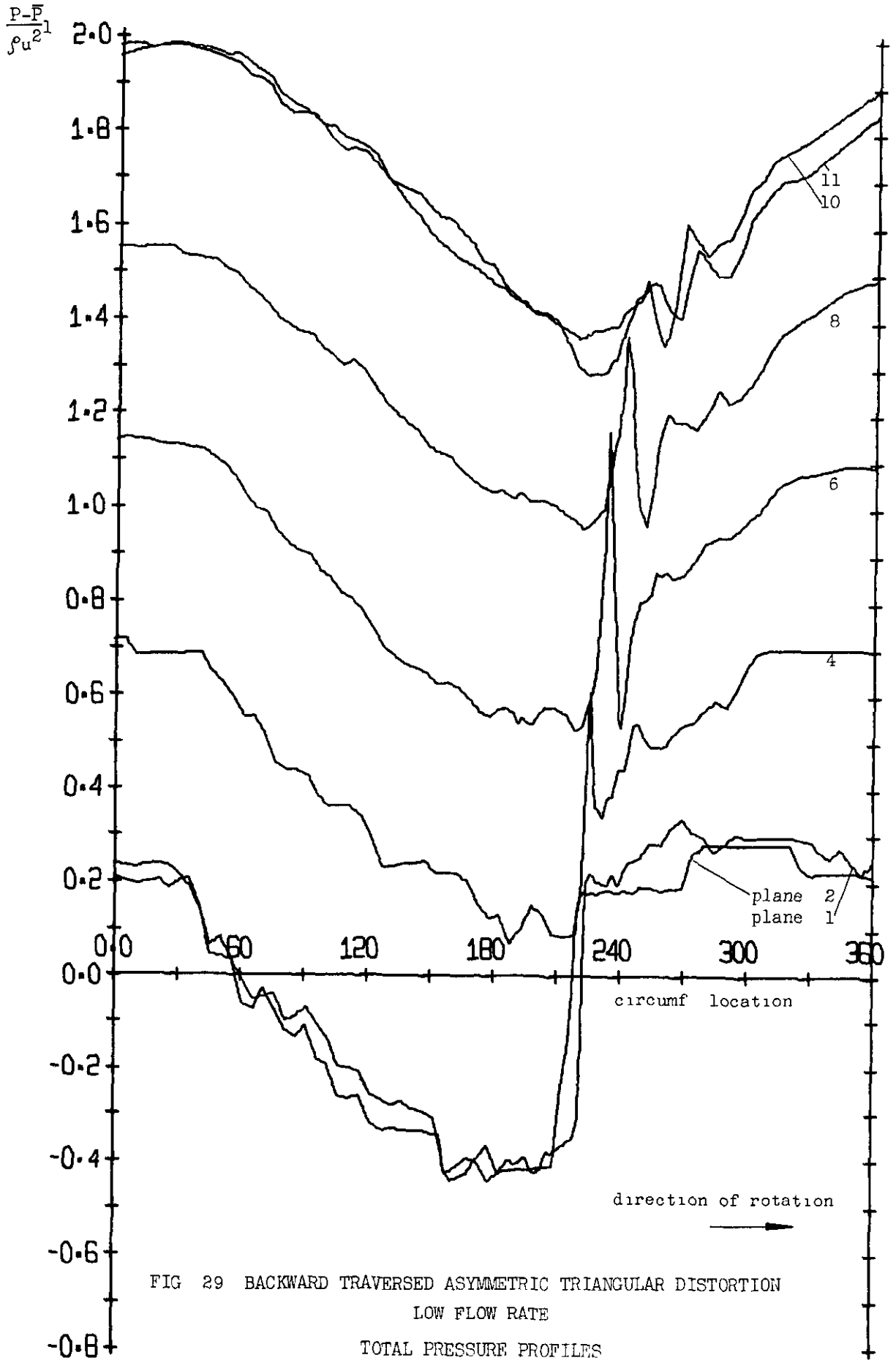

FIG 29 BACKWARD TRAVERSED ASYMMETRIC TRIANGULAR DISTORTION
LOW FLOW RATE
TOTAL PRESSURE PROFILES

FIG. 16 60° -SQUARE WAVE DISTORTION
LOW FLOW RATE
AXIAL VELOCITY PROFILES

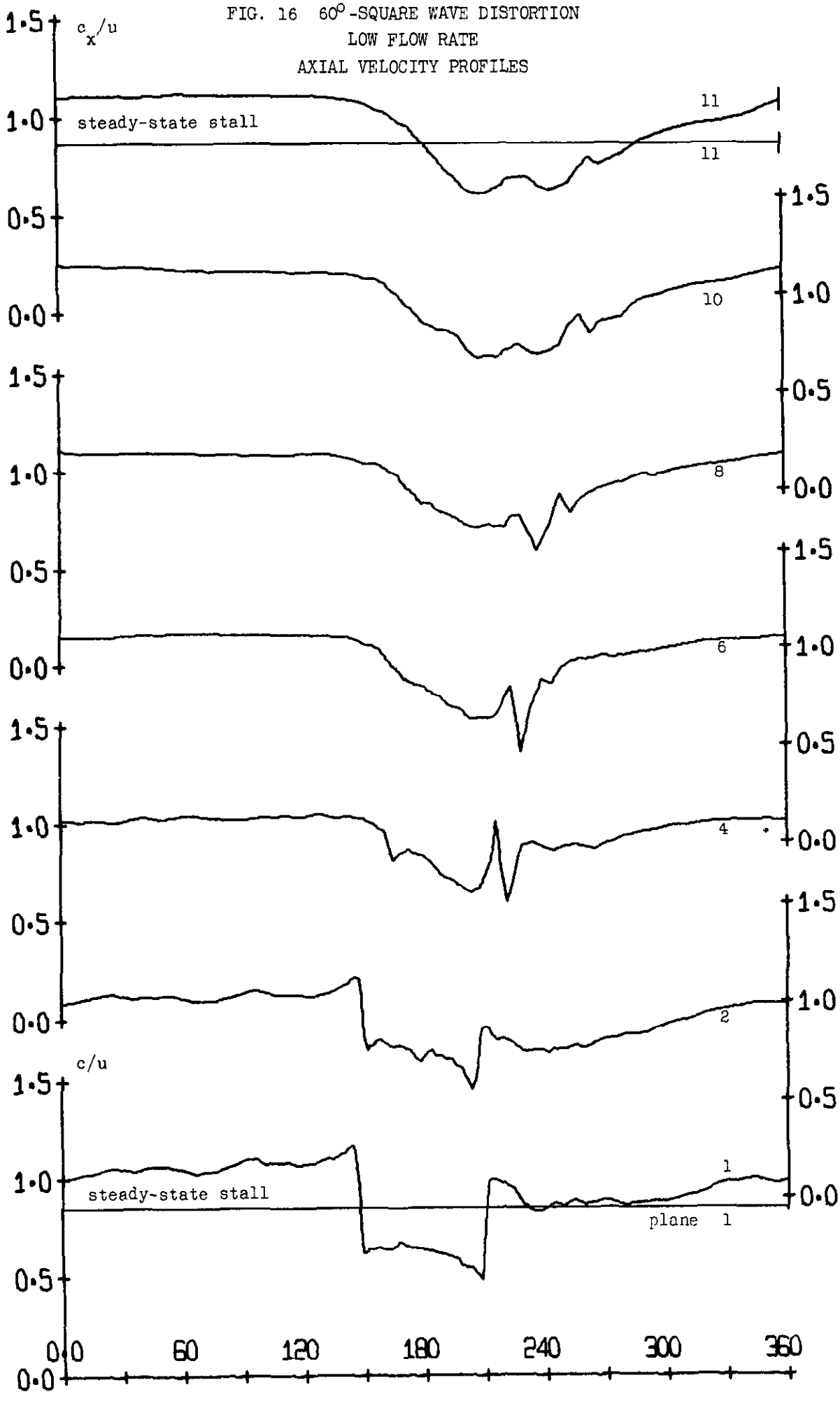

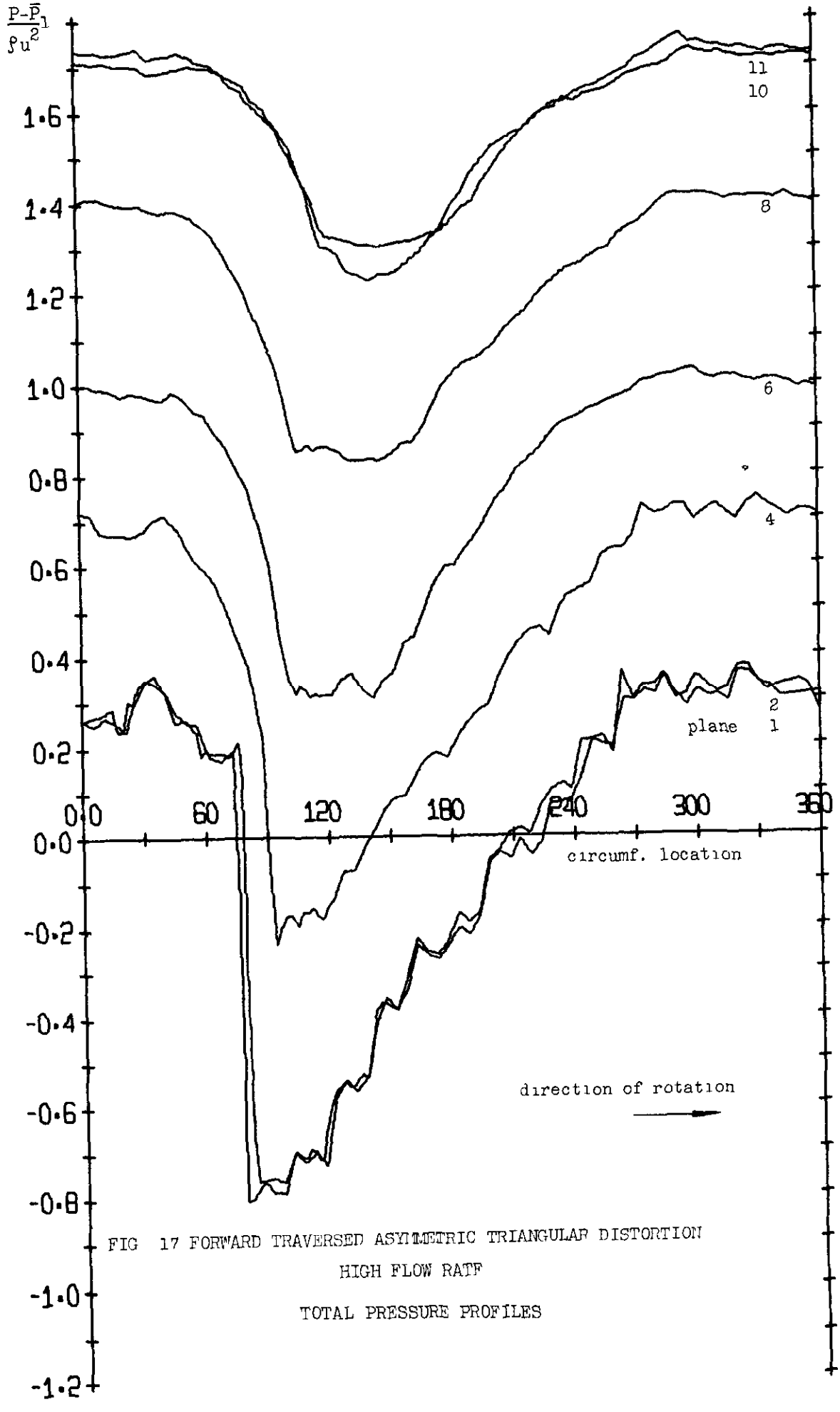

FIG 17 FORWARD TRAVERSED ASYMMETRIC TRIANGULAR DISTORTION

HIGH FLOW RATE

TOTAL PRESSURE PROFILES

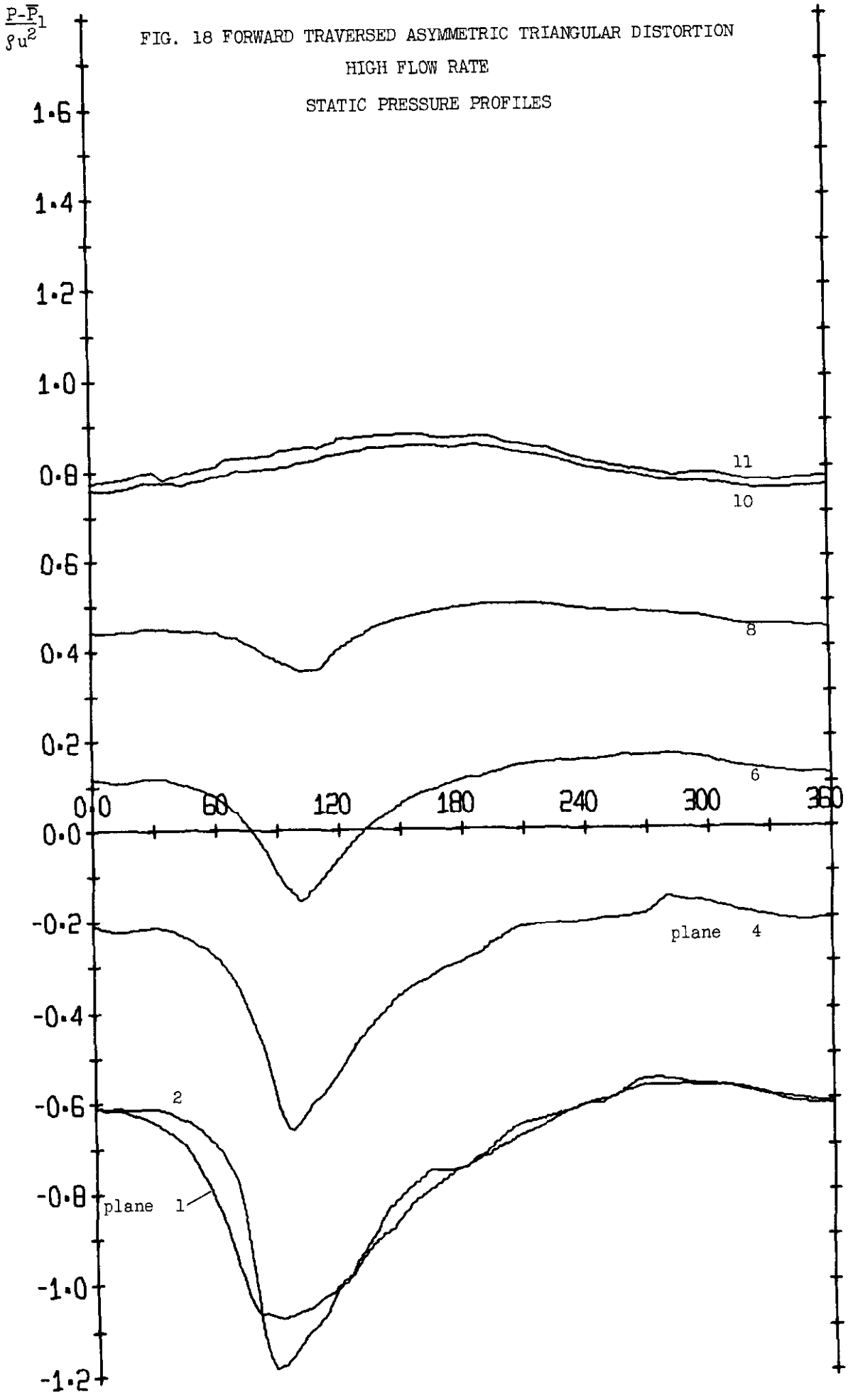
$\frac{P-\bar{P}_1}{\rho u^2}$
FIG. 18 FORWARD TRAVERSED ASYMMETRIC TRIANGULAR DISTORTION
HIGH FLOW RATE
STATIC PRESSURE PROFILES
1·6
1·4
1·2
1·0
0·8
0·6
0·4
0·2
0·0
-0·2
-0·4
-0·6
-0·8
-1·0
-1·2
0·0
60
120
180
240
300
360
11
10
8
6
plane 4
2
plane 1

FIG. 19 FORWARD TRAVERSED ASYMMETRIC TRIANGULAR DISTORTION
HIGH FLOW RATE FLOW ANGLES

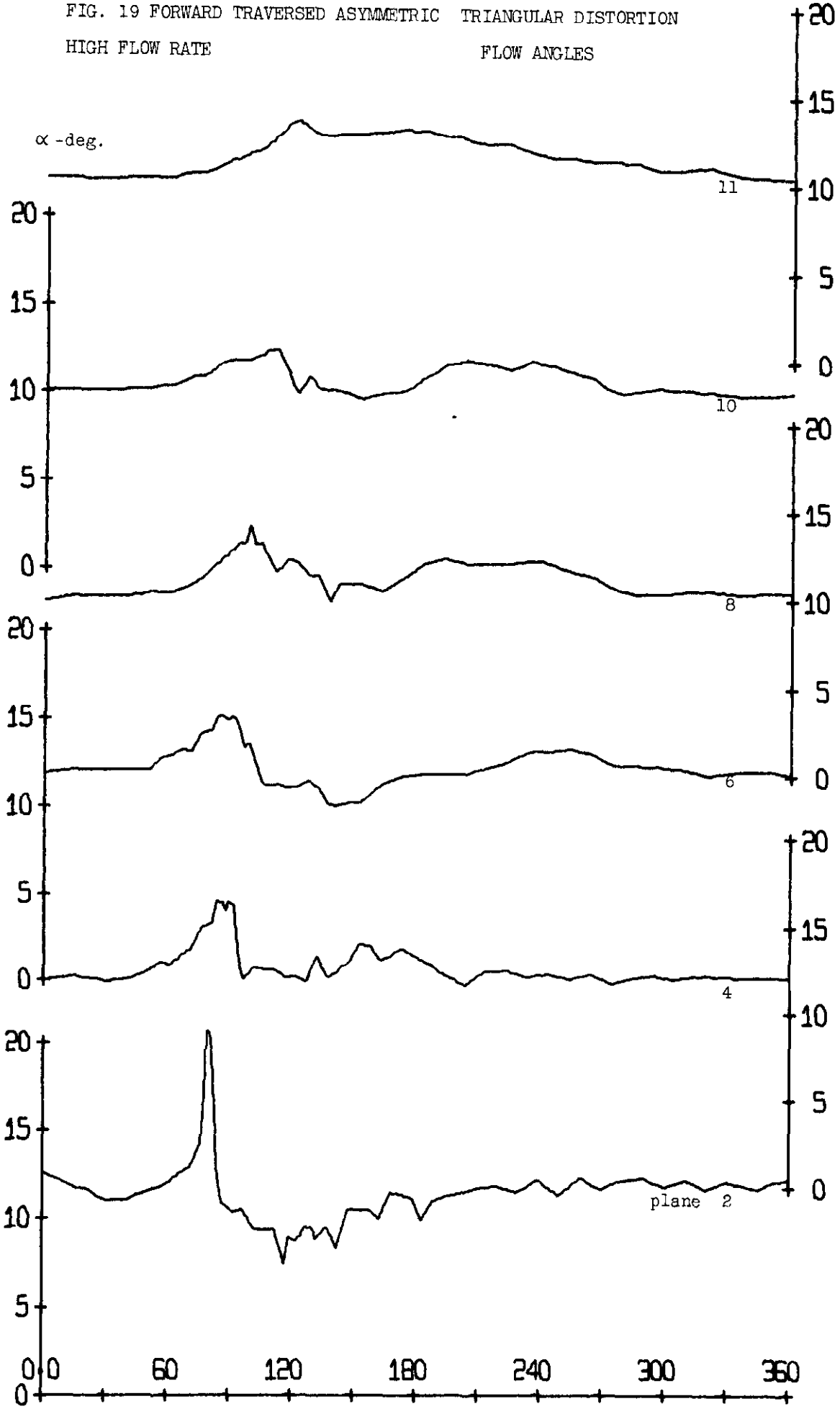

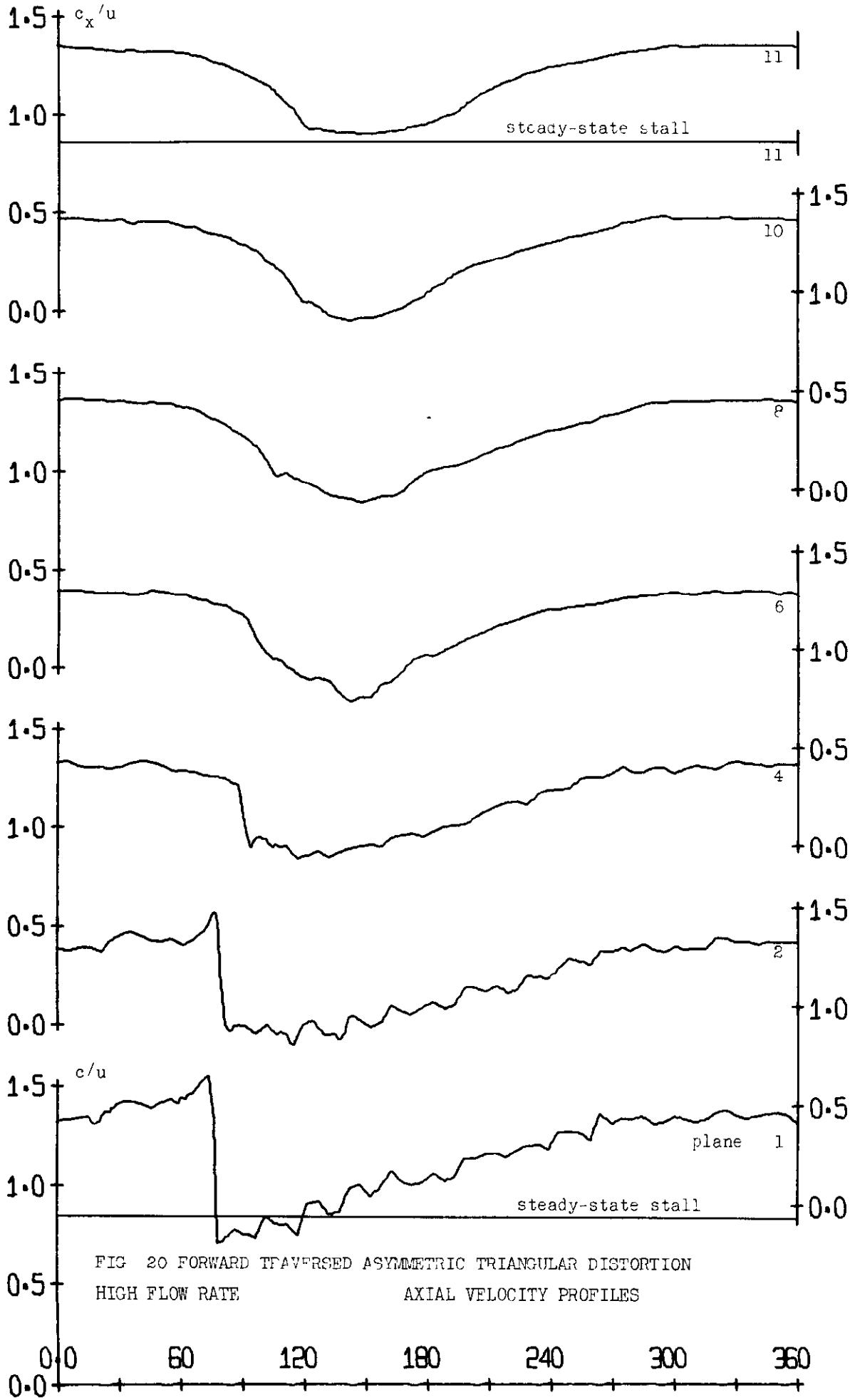

FIG 20 FORWARD TRAVERSED ASYMMETRIC TRIANGULAR DISTORTION
HIGH FLOW RATE AXIAL VELOCITY PROFILES

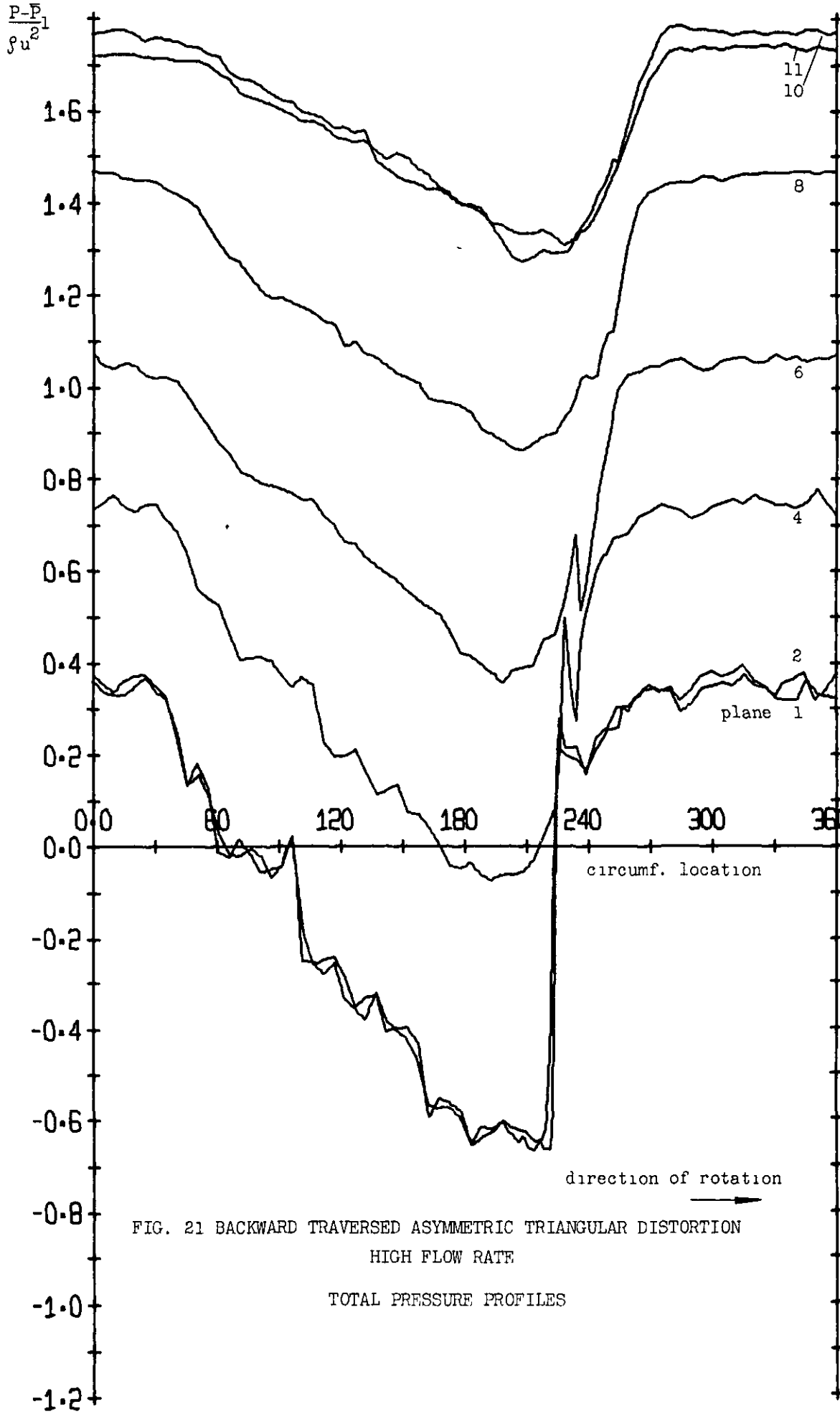

FIG. 21 BACKWARD TRAVERSED ASYMMETRIC TRIANGULAR DISTORTION

HIGH FLOW RATE

TOTAL PRESSURE PROFILES

FIG. 22 BACKWARD TRAVERSED ASYMMETRIC TRIANGULAR DISTORTION

HIGH FLOW RATE

STATIC PRESSURE PROFILES

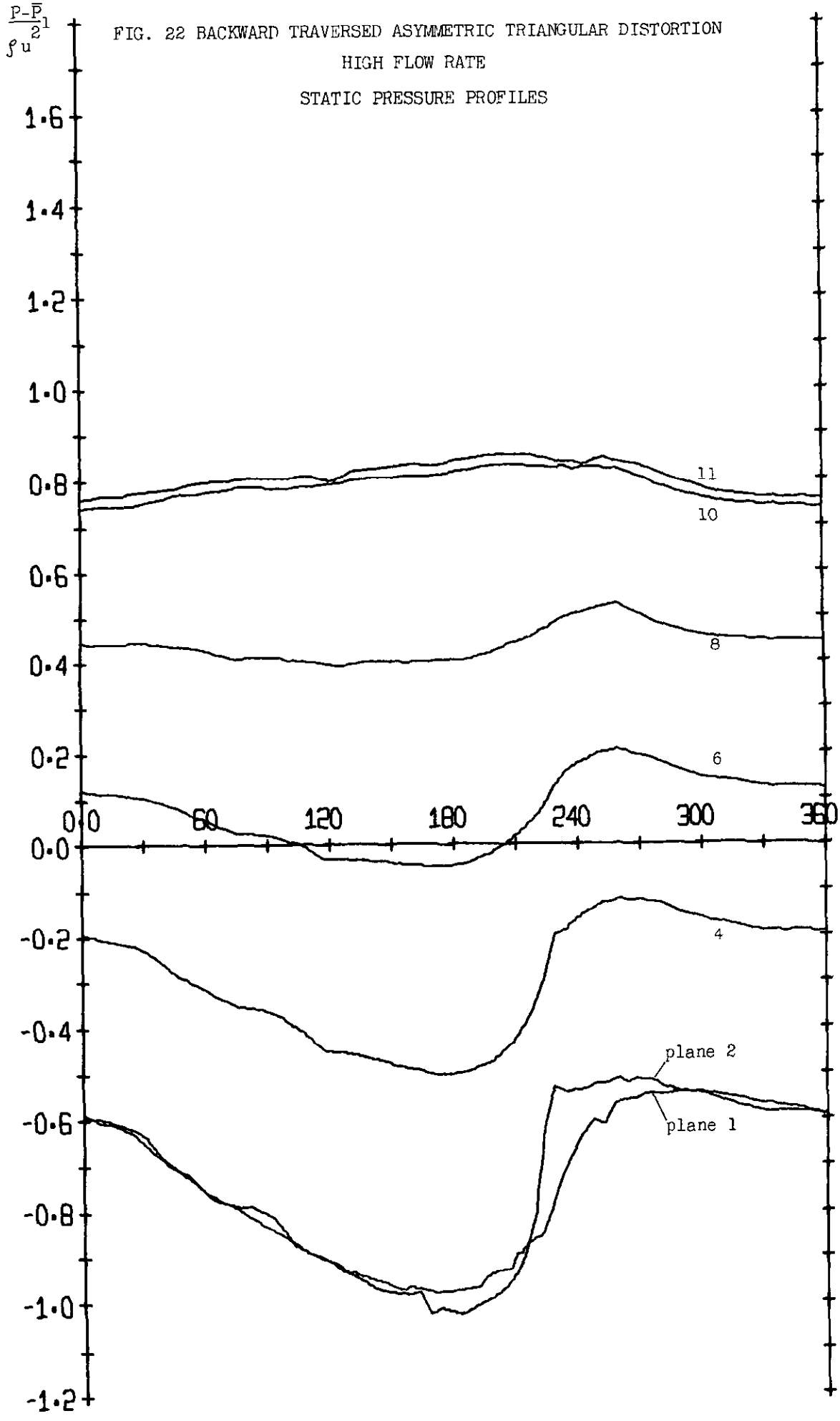

FIG 23 BACKWARD TRAVERSED ASYMMETRIC TRIANGULAR DISTORTION

HIGH FLOW RATE FLOW ANGLES

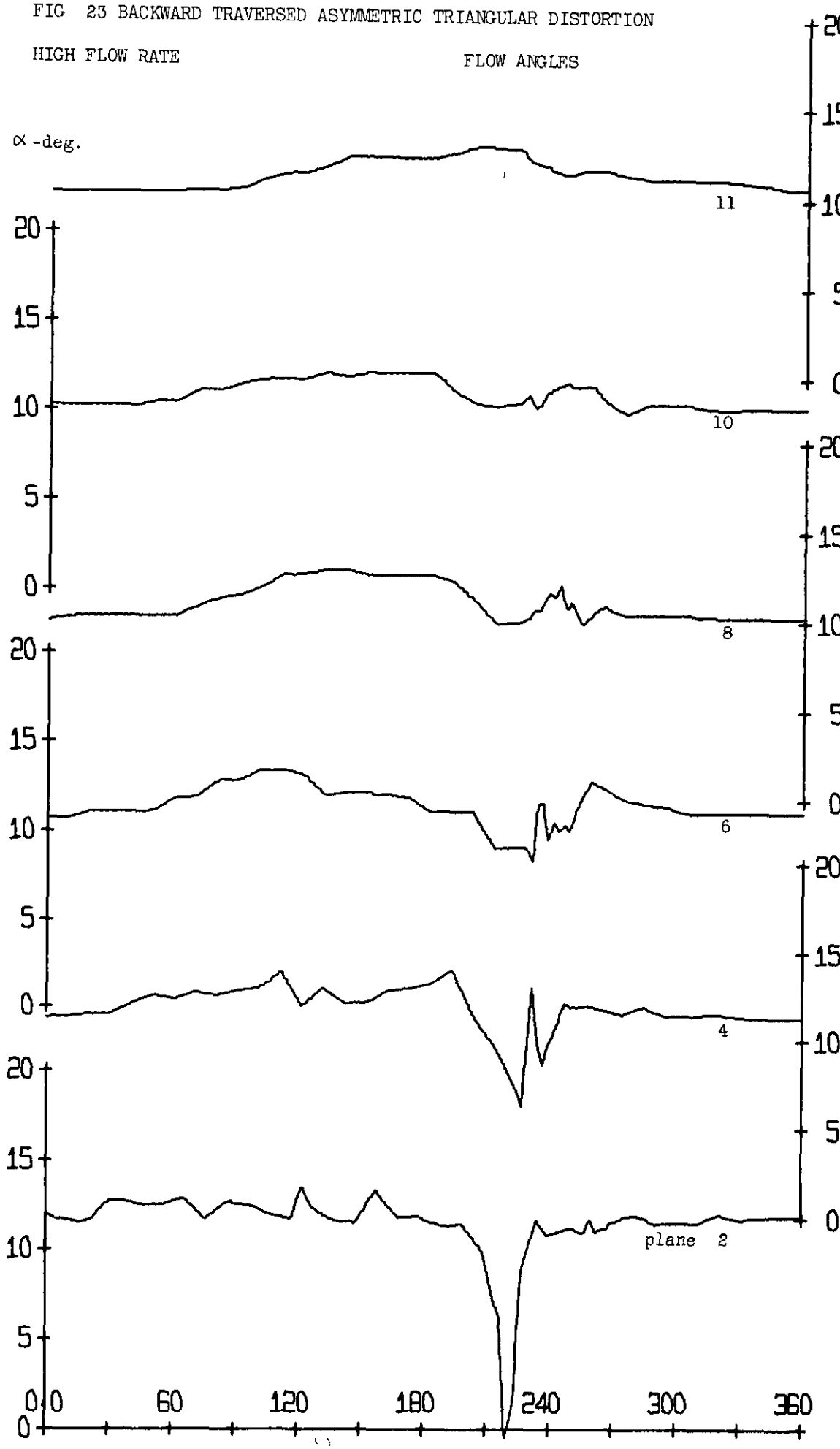

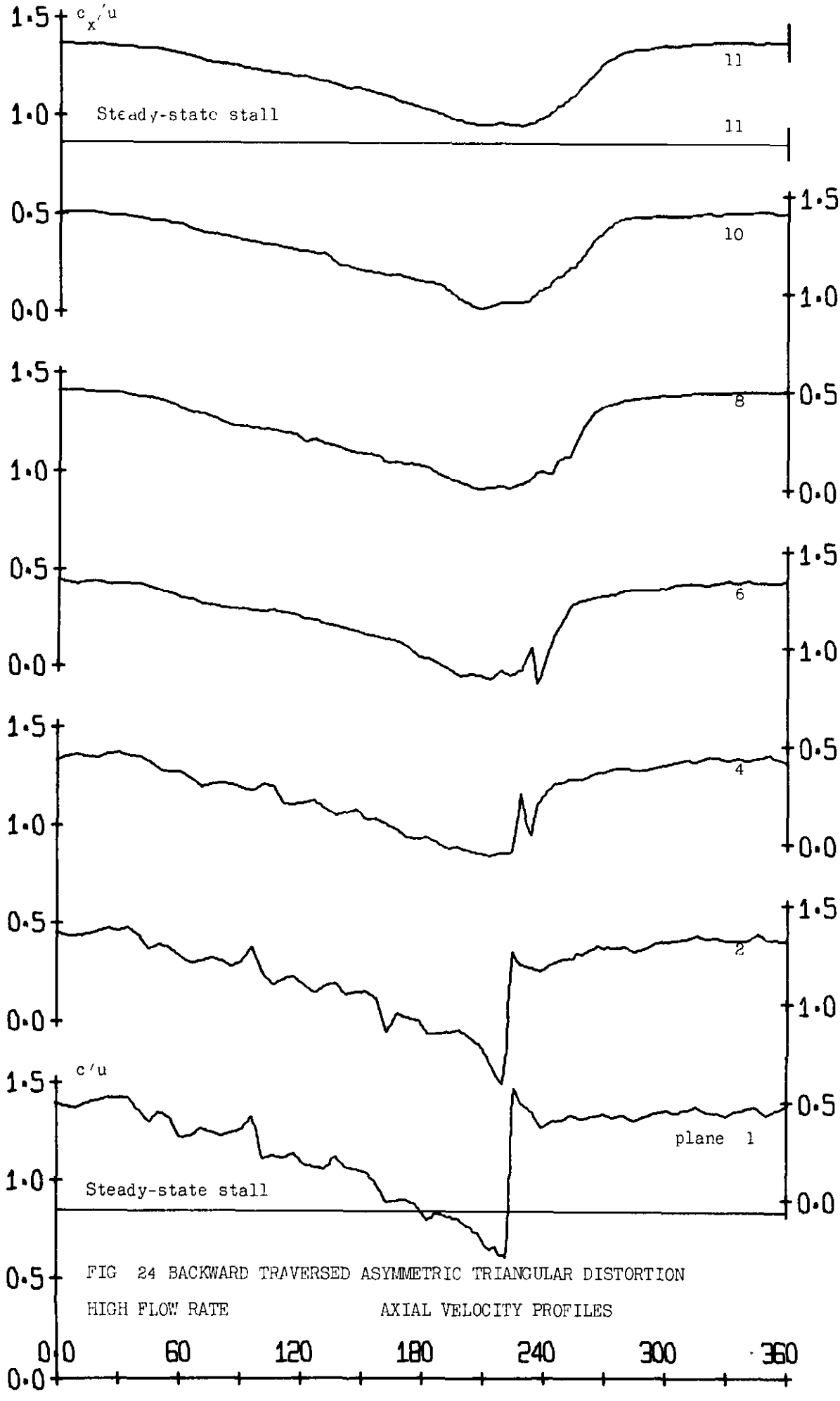

FIG 24 BACKWARD TRAVERSED ASYMMETRIC TRIANGULAR DISTORTION

HIGH FLOW RATE AXIAL VELOCITY PROFILES

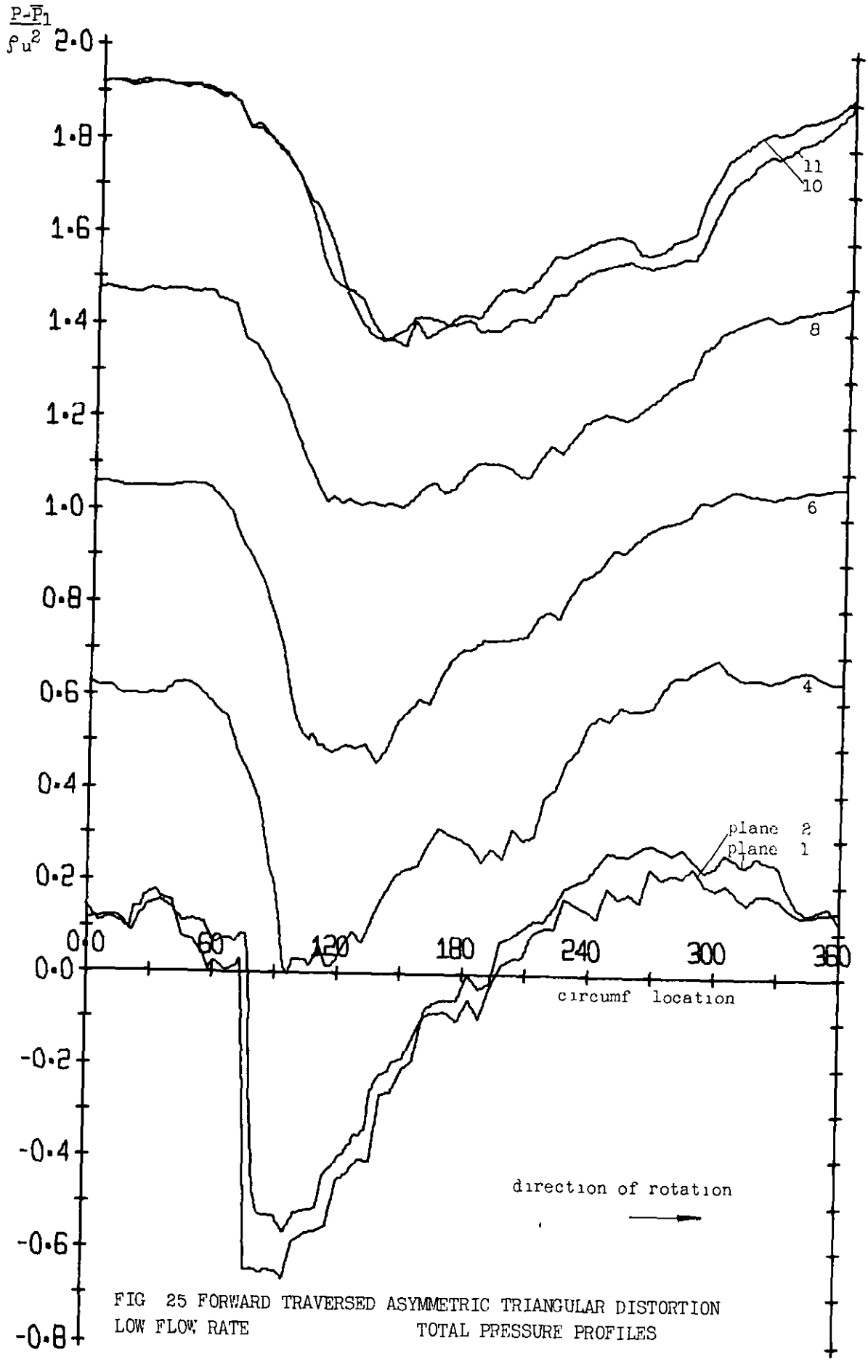

FIG 25 FORWARD TRAVERSED ASYMMETRIC TRIANGULAR DISTORTION
LOW FLOW RATE TOTAL PRESSURE PROFILES

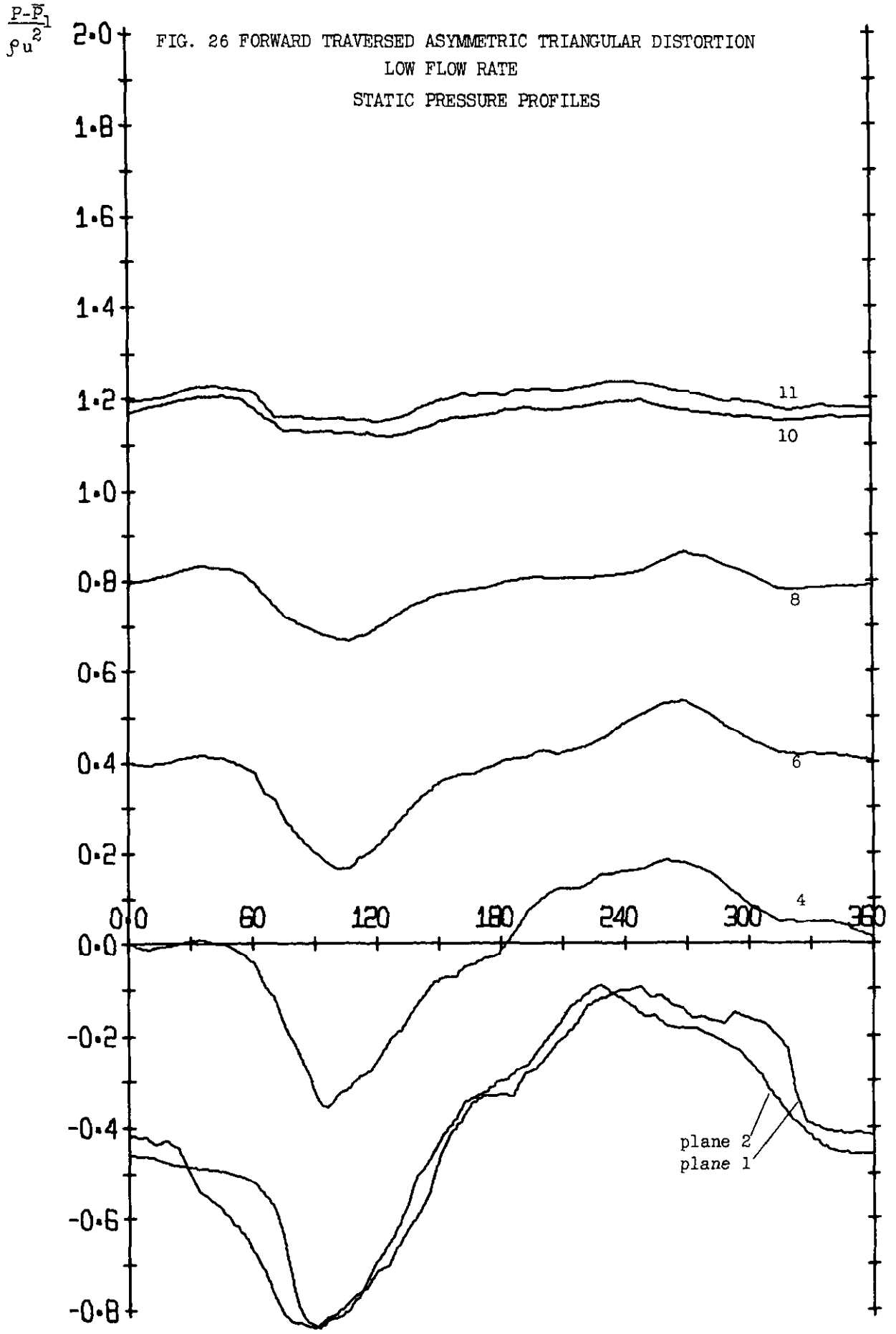
$\frac{P-\bar{P}_1}{\rho u^2}$
FIG. 26 FORWARD TRAVERSED ASYMMETRIC TRIANGULAR DISTORTION
LOW FLOW RATE
STATIC PRESSURE PROFILES
2·0
1·8
1·6
1·4
1·2
1·0
0·8
0·6
0·4
0·2
0·0
-0·2
-0·4
-0·6
-0·8
0·0
60
120
180
240
300
360
11
10
8
6
4
plane 2
plane 1

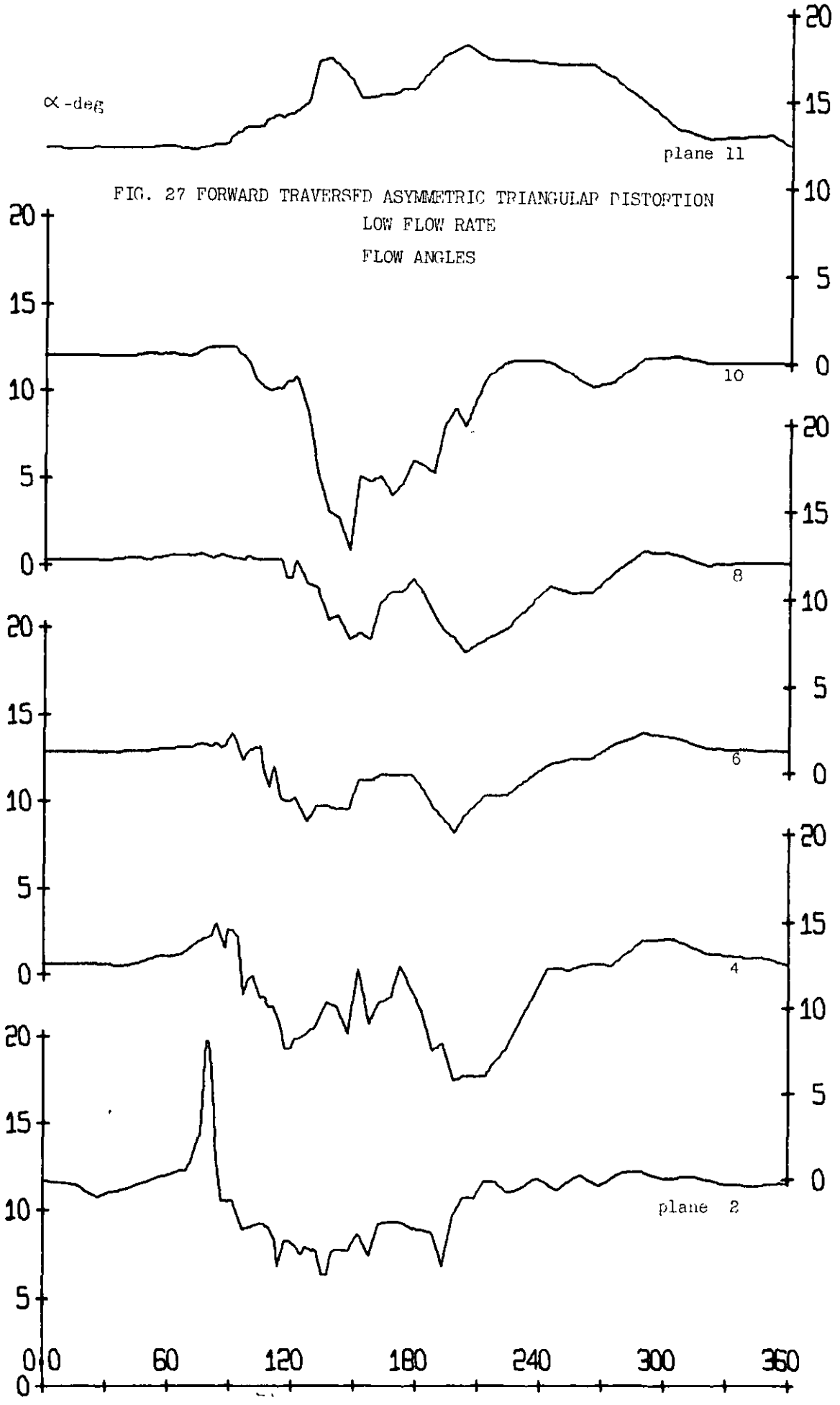

FIG. 27 FORWARD TRAVERSED ASYMMETRIC TRIANGULAR DISTORTION
LOW FLOW RATE
FLOW ANGLES

FIG. 28 FORWARD TRAVERSED ASYMMETRIC TRIANGULAR DISTORTION
AXIAL VELOCITY PROFILES
LOW FLOW RATE

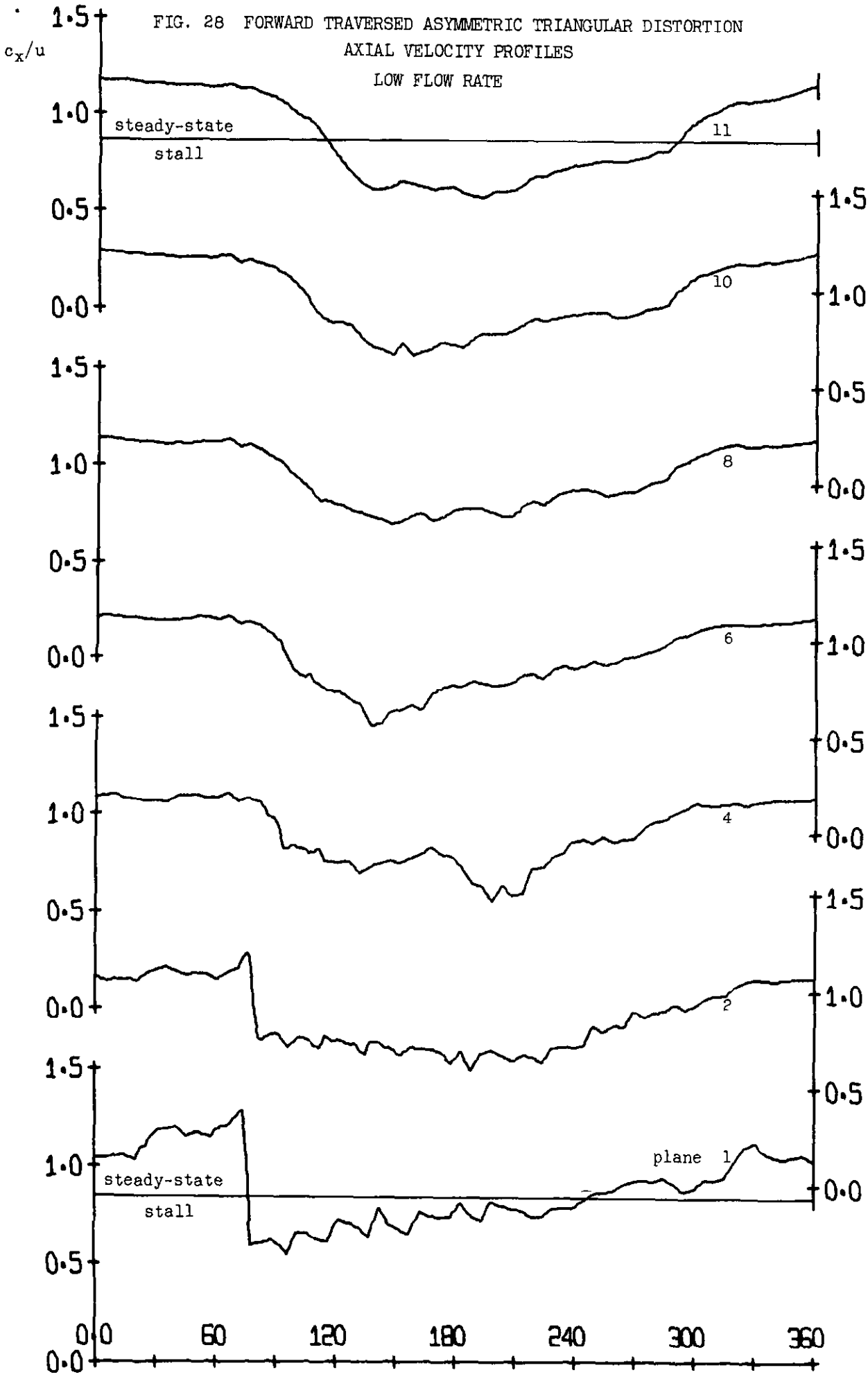

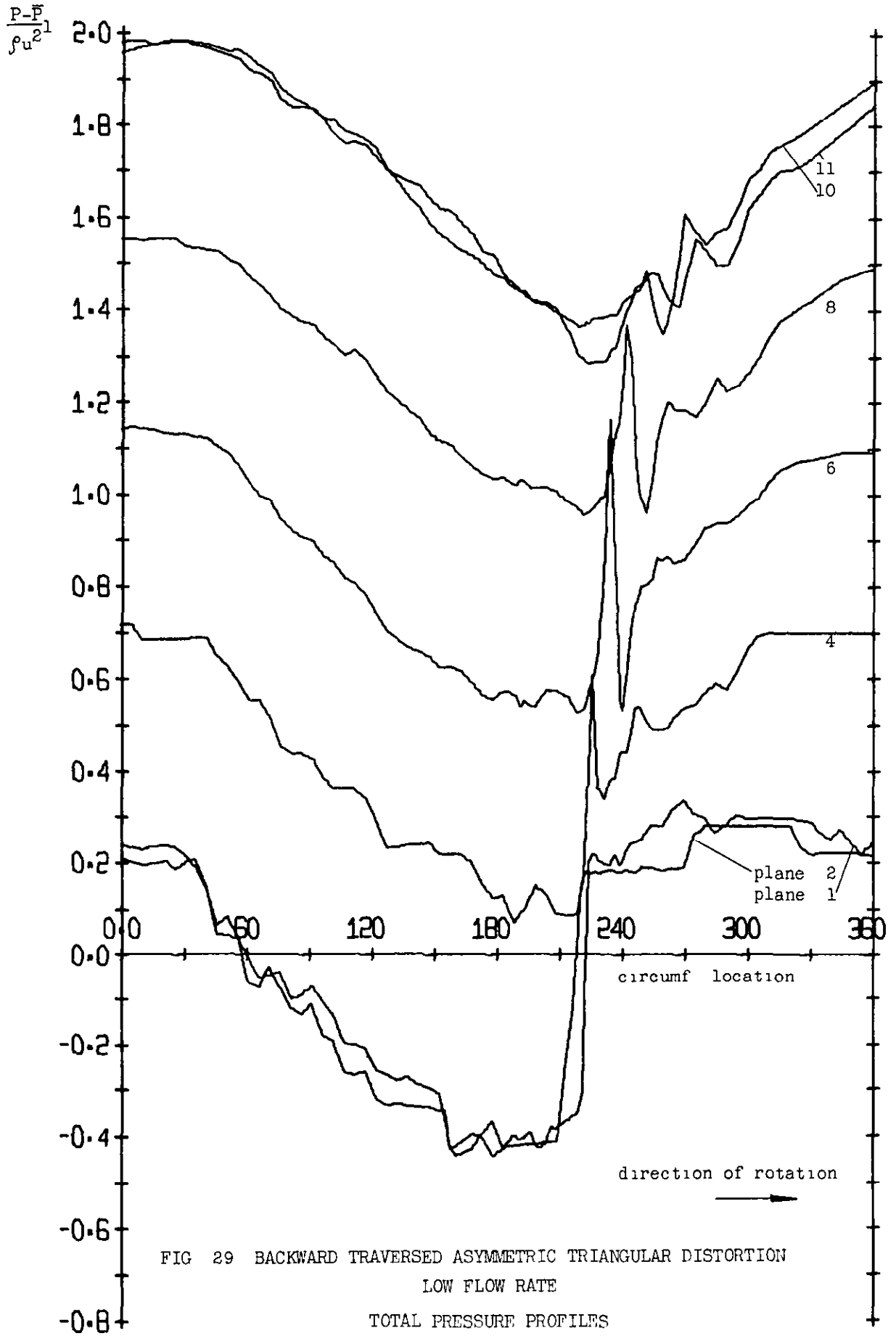

FIG 29 BACKWARD TRAVERSED ASYMMETRIC TRIANGULAR DISTORTION
LOW FLOW RATE
TOTAL PRESSURE PROFILES

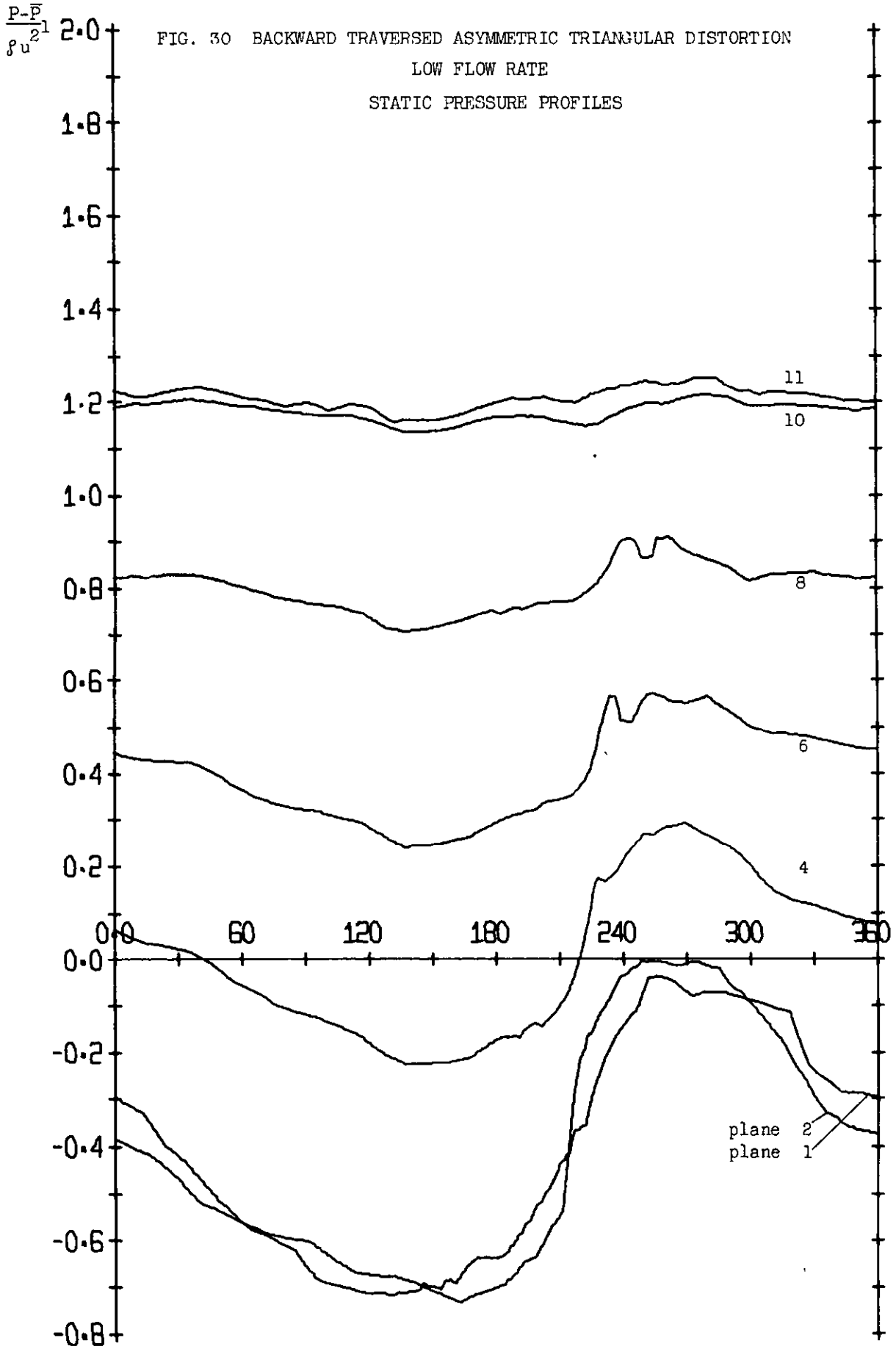

FIG. 30 BACKWARD TRAVERSED ASYMMETRIC TRIANGULAR DISTORTION
LOW FLOW RATE
STATIC PRESSURE PROFILES

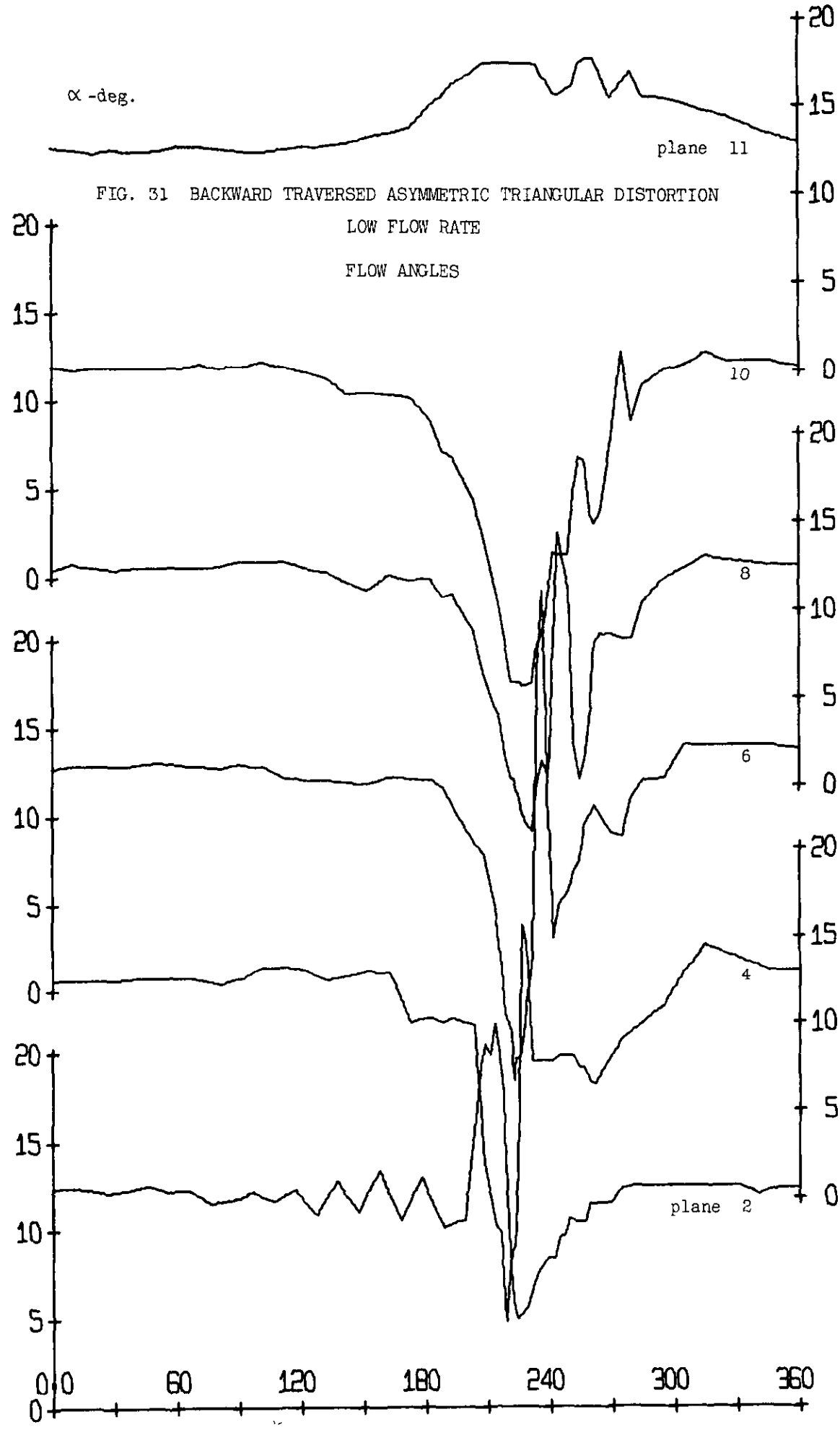

FIG. 31 BACKWARD TRAVERSED ASYMMETRIC TRIANGULAR DISTORTION
LOW FLOW RATE
FLOW ANGLES

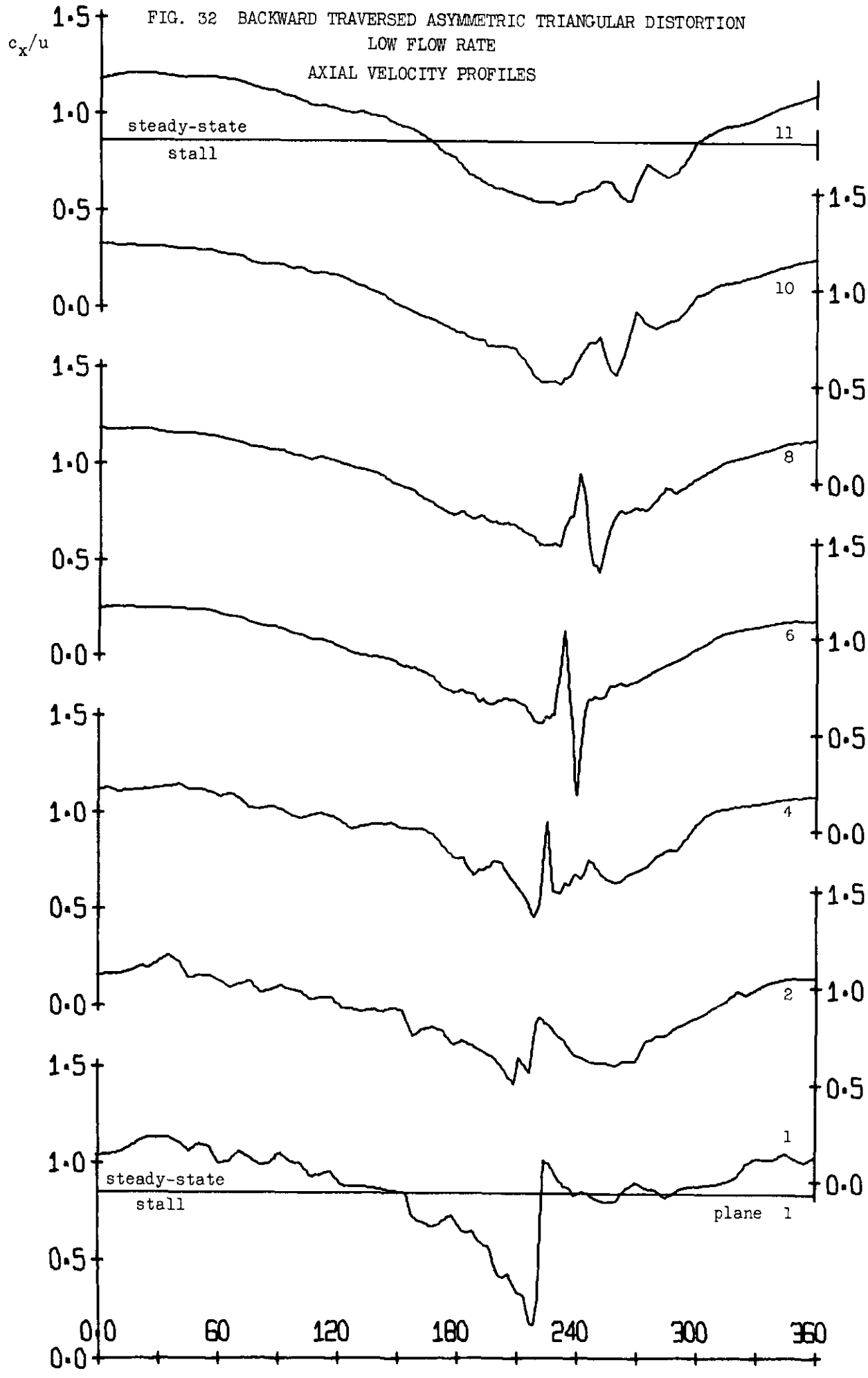
FIG. 32 BACKWARD TRAVERSED ASYMMETRIC TRIANGULAR DISTORTION
LOW FLOW RATE
AXIAL VELOCITY PROFILES
c_x/u
steady-state
stall
11
10
8
6
4
2
1
plane 1
1·5
1·0
0·5
0·0
0
60
120
180
240
300
360

HER MAJESTY'S STATIONERY OFFICE

Government Bookshops

49 High Holborn, London WC1V 6HB
13a Castle Street, Edinburgh EH2 3AR
109 St Mary Street, Cardiff CF1 1JW
Brazennose Street, Manchester M60 8AS
50 Fairfax Street, Bristol BS1 3DE
258 Broad Street, Birmingham B1 2HE
80 Chichester Street, Belfast BT1 4JY

Government publications are also available through booksellers

C.P. No. 1203

SBN 11 470471 6